

# The Spectral Barycentre of a Set of Graphs with Community Structure

François G. Meyer\*  
Applied Mathematics  
University of Colorado at Boulder, Boulder CO 80305  
[fmeyer@colorado.edu](mailto:fmeyer@colorado.edu)  
<https://francoismeyer.github.io>

August 21, 2025

## Abstract

The notion of barycentre graph is of crucial importance for machine learning algorithms that process graph-valued data. The barycentre graph is a “summary graph” that captures the mean topology and connectivity structure of a training dataset of graphs. The construction of a barycentre requires the definition of a metric to quantify distances between pairs of graphs. In this work, we use a multiscale spectral distance that is defined using the eigenvalues of the normalized graph Laplacian. The eigenvalues – but not the eigenvectors – of the normalized Laplacian of the barycentre graph can be determined from the optimization problem that defines the barycentre. In this work, we propose a structural constraint on the eigenvectors of the normalized graph Laplacian of the barycentre graph that guarantees that the barycentre inherits the topological structure of the graphs in the sample dataset. The eigenvectors can be computed using an algorithm that explores the large library of Soules bases. When the graphs are random realizations of a balanced stochastic block model, then our algorithm returns a barycentre that converges asymptotically (in the limit of large graph size) almost-surely to the population mean of the graphs. We perform Monte Carlo simulations to validate the theoretical properties of the estimator; we conduct experiments on real-life graphs that suggest that our approach works beyond the controlled environment of stochastic block models.

Keywords: Barycentre graph; Soules basis; Fréchet mean; Laplacian Spectral distance; statistical analysis of graph-valued data.

## 1 Introduction, problem statement, and related work

### 1.1 The barycentre graph

The design of machine learning algorithms that can analyze “graph-valued random variables” is of fundamental importance (e.g., [6, 7, 28, 45, 47, 48, 50, 56, 64, 83], and references therein). Such algorithms often require the computation of a “sample mean” graph that can summarize the topology and connectivity of a training dataset of graphs,  $\{\mathbf{G}^{(1)}, \dots, \mathbf{G}^{(T)}\}$ .

Formally, we denote by  $\mathcal{S}$  the set of  $\mathbf{n} \times \mathbf{n}$  symmetric adjacency matrices with nonnegative weights.

We equip  $\mathcal{S}$  with a probability  $\mathbb{P}$ . An example of a probability space  $(\mathcal{S}, \mathbb{P})$  is the stochastic block model (SBM), described in Section 1.8.

The adjacency matrix  $\mathbf{A}^{(t)}$  of the graph  $\mathbf{G}^{(t)}$ ,  $t = 1, \dots, T$  is sampled from  $(\mathcal{S}, \mathbb{P})$ . We equip  $(\mathcal{S}, \mathbb{P})$  with a metric  $\mathbf{d}$  to quantify proximity of graphs. A notion of summary graph is provided by the concept of *barycentre* [72], or *Fréchet*

---

\*FGM was supported in part by the National Science Foundation (CCF/CIF 1815971).

mean graph [10],  $\hat{\boldsymbol{\mu}}_{\mathcal{T}}[\mathbb{P}]$ , which minimizes the sum of the squared distances to all the graphs in the sample,

$$\hat{\boldsymbol{\mu}}_{\mathcal{T}}[\mathbb{P}] \stackrel{\text{def}}{=} \underset{\mathbf{B} \in \mathcal{S}}{\operatorname{argmin}} \sum_{t=1}^{\mathcal{T}} d^2(\mathbf{B}, \mathbf{A}^{(t)}). \quad (1)$$

Before continuing, we introduce some notations. We denote by  $[\mathbf{n}] \stackrel{\text{def}}{=} \{1, \dots, \mathbf{n}\}$ . We define  $\mathbf{1} \stackrel{\text{def}}{=} [1 \cdots 1]^{\top}$ , and  $\mathbf{J} = \mathbf{1}\mathbf{1}^{\top}$ . We use  $\mathbf{A}$  to denote the adjacency matrix of a graph  $\mathbf{G}$ , and  $\mathbf{D} \stackrel{\text{def}}{=} \operatorname{diag}(\mathbf{A}\mathbf{1})$  to denote the diagonal degree matrix. The symmetric normalized adjacency matrix,  $\hat{\mathbf{A}} = \mathbf{D}^{-1/2}\mathbf{A}\mathbf{D}^{-1/2}$ , is defined by

$$\hat{a}_{ij} \stackrel{\text{def}}{=} a_{ij}/\sqrt{d_i d_j} \text{ if } d_i d_j \neq 0; \text{ and } \hat{a}_{ij} \stackrel{\text{def}}{=} 0 \text{ otherwise.} \quad (2)$$

The normalized Laplacian is defined by  $\mathcal{L} \stackrel{\text{def}}{=} \operatorname{Id} - \hat{\mathbf{A}}$ . We denote by  $\boldsymbol{\lambda}(\mathcal{L}) = [\lambda_1, \dots, \lambda_n]$  the ascending sequence of eigenvalues of  $\mathcal{L}$ ,  $0 = \lambda_1 \leq \dots \leq \lambda_n \leq 2$ .

## 1.2 The Laplacian spectral pseudo-distance

The metric  $\mathbf{d}$  in Eq. (1) influences the topological characteristics that  $\hat{\boldsymbol{\mu}}_{\mathcal{T}}[\boldsymbol{\mu}]$  inherits from  $\{\mathbf{G}^{(1)}, \dots, \mathbf{G}^{(\mathcal{T})}\}$  [59]. We advocate that the distance between graphs should be evaluated in the spectral domain, by comparing the eigenvalues of the normalized Laplacian,  $\mathcal{L}^{(t)}$ , of the respective graphs  $\mathbf{G}^{(t)}$ . We define the Laplacian spectral pseudo-metric between two graphs  $\mathbf{G}$  and  $\mathbf{G}'$  by

$$\mathbf{d}(\mathcal{L}, \mathcal{L}') \stackrel{\text{def}}{=} \|\boldsymbol{\lambda}(\mathcal{L}) - \boldsymbol{\lambda}(\mathcal{L}')\|_2, \quad (3)$$

where  $\boldsymbol{\lambda}(\mathcal{L})$  and  $\boldsymbol{\lambda}(\mathcal{L}')$  are the vectors of eigenvalues of  $\mathcal{L}$  and  $\mathcal{L}'$  respectively. This pseudo-distance captures at multiple scales the structural and connectivity in the graphs (e.g., diameter, number of connected components, clusterability, diffusion distance, [17, 19, 27, 77]). Defining a pseudo-distance in the spectral domain alleviates the difficulty of solving the node correspondence problem, and in the case of the normalized Laplacian, it makes it possible to compare graphs of different sizes. When the graphs are realizations of a stochastic block model, the eigenvalues of  $\mathcal{L}$  associated with each community are better separated from the bulk (see Fig. 2 for a real-life instance of this fact) than the corresponding eigenvalues of  $\mathbf{L} \stackrel{\text{def}}{=} \mathbf{D} - \mathbf{A}$  [23].

## 1.3 The spectrum of the barycentre graph

In spite of the advantages of the pseudo-metric  $\mathbf{d}$  defined by Eq. (3), the computation of the solution to Eq. (1) leads to two technical obstacles. The first challenge stems from the fact that  $\mathbf{d}$  is defined in the spectral domain, but the optimization Eq. (1) takes place in  $\mathcal{S}$  [40]. This leads to the definition of a *realizable* sequence; we say that  $\boldsymbol{\lambda} = [\lambda_1, \dots, \lambda_n]$  is realizable if there exists  $\mathbf{A} \in \mathcal{S}$  whose Laplacian,  $\mathcal{L}(\mathbf{A})$ , satisfies  $\boldsymbol{\lambda}(\mathcal{L}(\mathbf{A})) = \boldsymbol{\lambda}$ . Hereinafter, we define  $\mathcal{R}$  to be the *set of realizable sequences*. We can formalize the optimisation problem associated with the estimation of  $\hat{\boldsymbol{\mu}}_{\mathcal{T}}[\mathbb{P}]$  in Eq. (1),

$$\boldsymbol{\lambda}(\mathcal{L}(\hat{\boldsymbol{\mu}}_{\mathcal{T}}[\mathbb{P}])) = \underset{\boldsymbol{\lambda} \in \mathcal{R}}{\operatorname{argmin}} \sum_{t=1}^{\mathcal{T}} \|\boldsymbol{\lambda} - \boldsymbol{\lambda}(\mathcal{L}^{(t)})\|_2^2. \quad (4)$$

If we relax this minimization problem ( $\boldsymbol{\lambda} \in \mathbb{R}^n$ , instead of  $\boldsymbol{\lambda} \in \mathcal{R}$ ), then the solution to Eq. (4) is the sample mean  $\hat{\mathbb{E}}_{\mathcal{T}}[\boldsymbol{\lambda}] \stackrel{\text{def}}{=} \mathcal{T}^{-1} \sum_{t=1}^{\mathcal{T}} \boldsymbol{\lambda}(\mathcal{L}^{(t)})$ , which has no guarantee to be realizable. Which brings us to the second difficulty in using a spectral pseudo-distance.

## 1.4 The normalized Laplacian of the barycentre graph

The knowledge of the eigenvalues  $\boldsymbol{\lambda}(\mathcal{L}(\hat{\boldsymbol{\mu}}_{\mathcal{T}}[\mathbb{P}]))$  solution to Eq. (4) is insufficient to reconstruct the adjacency matrix of the barycentre graph  $\hat{\boldsymbol{\mu}}_{\mathcal{T}}[\mathbb{P}]$ ; we need an orthonormal basis of eigenvectors,  $\boldsymbol{\Psi} = [\boldsymbol{\psi}_1 \cdots \boldsymbol{\psi}_n]$  to compute

$$\mathcal{L}(\hat{\boldsymbol{\mu}}_{\mathcal{T}}[\mathbb{P}]) = \boldsymbol{\Psi} \operatorname{diag}(\hat{\mathbb{E}}_{\mathcal{T}}[\boldsymbol{\lambda}]) \boldsymbol{\Psi}^{\top}. \quad (5)$$

In addition to the constraint,  $\Psi \in O(\mathbf{n})$ , where  $O(\mathbf{n})$  is the orthogonal group, we need to make sure that  $[\psi_1 \ \cdots \ \psi_n]$  are the eigenvectors of a valid normalized Laplacian, to wit

$$\exists \mathbf{A} \in \mathcal{S}, \quad \Psi \text{diag}(\widehat{\mathbb{E}}_{\mathbb{T}}[\lambda]) \Psi^T = \text{Id} - \mathbf{D}^{-1/2} \mathbf{A} \mathbf{D}^{-1/2}, \quad (6)$$

where  $\mathbf{D} = \text{diag}(\mathbf{A}\mathbf{1})$ . When  $\Psi$  complies with Eq. (6), we can take the adjacency matrix of the barycentre graph to be

$$\widehat{\mu}_{\mathbb{T}}[\mathbb{P}] = \mathbf{D}^{1/2} [\text{Id} - \Psi \text{diag}(\widehat{\mathbb{E}}_{\mathbb{T}}[\lambda]) \Psi^T] \mathbf{D}^{1/2}. \quad (7)$$

### 1.5 The adjacency matrix of the barycentre graph: a structural constraint

In general the barycentre  $\widehat{\mu}_{\mathbb{T}}[\mathbb{P}]$  given by Eq. (7), for some random choice of  $\Psi \in O(\mathbf{n})$ , may have a very different topological structure than the graphs  $\{\mathbf{G}^{(1)}, \dots, \mathbf{G}^{(T)}\}$ . We would like to enforce the fact that  $\widehat{\mu}_{\mathbb{T}}[\mathbb{P}]$  should share the same topology and connectivity as  $\mathbb{E}[\mathbb{P}]$ . This requirement is well founded since  $\mathbb{E}[\mathbb{P}]$  captures the structural connectivity of the random graph ensemble defined by  $\mathbb{P}$ . For instance, if  $\mathbb{E}[\mathbb{P}]$  contains structures such as modular communities, rich clubs, hubs, trees, etc. we expect these structures to be present in  $\widehat{\mu}_{\mathbb{T}}[\mathbb{P}]$ .

This structural constraint can be formalized in the following way: we request that  $\widehat{\mu}_{\mathbb{T}}[\mathbb{P}]$  converges (as  $\mathbf{n} \rightarrow +\infty$ ) to  $\mathbb{E}[\mathbb{P}]$ , with high probability (asymptotically almost-surely). Formally, we require

$$\lim_{\mathbf{n} \rightarrow +\infty} \mathbb{P}(\widehat{\mu}_{\mathbb{T}}[\mathbb{P}] = \mathbb{E}[\mathbb{P}]) = 1. \quad (8)$$

We note in passing, that the trivial choice  $\widehat{\mu}_{\mathbb{T}}[\mathbb{P}] = \widehat{\mathbb{E}}_{\mathbb{T}}[\mathbb{P}]$ , where

$$[\widehat{\mathbb{E}}_{\mathbb{T}}[\mathbb{P}]]_{ij} \stackrel{\text{def}}{=} T^{-1} \sum_{t=1}^T a_{ij}^{(t)}, \quad (9)$$

does not satisfy the constraint given by Eq. (4), since in general we have  $\lambda(\widehat{\mathbb{E}}_{\mathbb{T}}[\mathbb{P}]) \neq \widehat{\mathbb{E}}_{\mathbb{T}}[\lambda]$  [5, 15].

Because the topological structures present in a graph are independent of the normalization of  $\mathbf{A}$ , we can replace  $\mathbf{A}$  with its symmetric normalized version  $\widehat{\mathbf{A}}$  (defined by Eq. (2)), or equivalently we can work with the normalized Laplacian of  $\mathbb{E}[\mathbb{P}]$ ,

$$\overline{\mathcal{L}} \stackrel{\text{def}}{=} \mathcal{L}(\mathbb{E}[\mathbb{P}]) = \text{Id} - [\overline{\mathbf{D}}]^{-1/2} \mathbf{P} [\overline{\mathbf{D}}]^{-1/2}, \quad (10)$$

where

$$\mathbf{P} \stackrel{\text{def}}{=} \mathbb{E}[\mathbb{P}], \quad \text{and} \quad \overline{\mathbf{D}} \stackrel{\text{def}}{=} \mathbb{E}[\mathbf{D}]. \quad (11)$$

Our definition of  $\overline{\mathcal{L}}$  is in agreement with others who have used this matrix to derive bounds on the concentration of  $\mathcal{L}$  [2, 51, 55, 62, 66]. On this account, we replace the asymptotic structural constraint given by Eq. (8) with

$$\lim_{\mathbf{n} \rightarrow +\infty} \mathbb{P}(\mathcal{L}(\widehat{\mu}_{\mathbb{T}}[\mathbb{P}]) = \overline{\mathcal{L}}) = 1. \quad (12)$$

### 1.6 Formulation of the problem

We combine Eq. (5) and Eq. (12), with the constraint that  $\Psi \in O(\mathbf{n})$  to get the following problem: given  $\widehat{\mathbb{E}}_{\mathbb{T}}[\lambda]$ , find  $\Psi \in O(\mathbf{n})$  such that

$$\lim_{\mathbf{n} \rightarrow +\infty} \mathbb{P}(\Psi \text{diag}(\widehat{\mathbb{E}}_{\mathbb{T}}[\lambda]) \Psi^T = \overline{\mathcal{L}}) = 1. \quad (13)$$

In this work, we prove that it is possible to solve this problem using a “customized” Soules basis  $\Psi$ . We prove that when  $(\mathcal{S}, \mathbb{P})$  is the probability space associated with a balanced stochastic block model, then  $\widehat{\mu}_{\mathbb{T}}[\mathbb{P}] = \mathbb{E}[\mathbb{P}]$  asymptotically almost-surely, where  $\widehat{\mu}_{\mathbb{T}}[\mathbb{P}]$  is defined by Eq. (7).

## 1.7 State of the art

The requirement given by Eq. (13) can be approximately achieved if  $\Psi$  is an “average on  $O(\mathbf{n})$ ” of the distribution of bases of eigenvectors associated with the respective Laplacian matrices  $\mathcal{L}^{(t)}$  of the graphs in the sample. To this goal several authors have proposed to align the eigenvectors of the respective graph adjacency matrices [37] or Laplacian matrices [76]. Rather than working with the eigenvalues of the normalized Laplacian, the authors in [46] seek the barycentre graph on the cone of symmetric positive semidefinite matrices. They characterize the space of graph Laplacians, a subset of this cone, to develop statistical tests about the location of the Fréchet mean. Others [36] have proposed numerical methods to find the best stochastic block model (SBM) whose eigenvalues match the sample mean eigenvalues.

## 1.8 The stochastic block model

Experiments performed on random graph ensembles, with adjustable parameters, provide a mechanism to quantify the performance of graph-valued algorithms [63]. To provide theoretical guarantees for the algorithms presented in this paper, we analyse the algorithms when the graphs are sampled from a random graph model: the stochastic block model (e.g., [1], and references therein).

In the next subsections, we define the stochastic block model, justify the importance of this model, and give an example of a real-life dynamic graph that will be studied in detail in Section 6.2.

### 1.8.1 Definition

We define the general stochastic block model  $\text{SBM}(\mathbf{p}, \mathbf{q}, \mathbf{n})$ . Let  $\{\mathbf{B}_k\}$ ,  $1 \leq k \leq M$  be a partition of the vertex set  $[\mathbf{n}]$  into  $M$  blocks (or communities). We define the vector  $\mathbf{p} = [\mathbf{p}_1 \cdots \mathbf{p}_M]$  to be the edge probabilities within each block, and  $\mathbf{q}$  to be the edge probability between blocks. The entries  $\mathbf{a}_{ij} = \mathbf{a}_{ji}$ ,  $i < j$  of the adjacency matrix  $\mathbf{A}$  are independent (up to symmetry) and are distributed with Bernoulli distributions with parameter  $\mathbf{p}_m$  if  $i$  and  $j$  are in the same block  $\mathbf{B}_m$ , and parameter  $\mathbf{q}$  if  $i$  and  $j$  are in distinct blocks.

We often represent  $\text{SBM}(\mathbf{p}, \mathbf{q}, \mathbf{n})$  by the matrix of edge probabilities, or matrix of connection probabilities,  $\mathbf{P}$  defined by Eq. (11). We sometimes consider a balanced version of the model where all blocks have the same size,  $|\mathbf{B}_m| = \mathbf{n}/M$ , (in that case we assume without loss of generality that  $\mathbf{n}$  is a multiple of  $M$ ), and all the edge probabilities are equal,  $\mathbf{p}_1 = \cdots = \mathbf{p}_M$ . We denote this probability space by  $\text{SBM}(\mathbf{p}, \mathbf{q}, \mathbf{n})$ , since  $\mathbf{p}$  is a scalar and no longer a vector.

### 1.8.2 Motivation for using stochastic block models

The stochastic block model represents the quintessential exemplar of a graph with community structure. It has been used extensively in the study of complex real-life graphs [35, 74]. Stochastic block models have also been shown to provide universal approximants (under various norms or distances) (e.g., [3, 36, 44, 61] and references therein), and can therefore be used as building blocks to analyse more complex

graphs. In fact, it was shown in [81] that the structural analysis of a large graph is equivalent to the approximation of that graph using stochastic block models, of decreasing complexity as the scale of the analysis becomes coarser.

Stochastic block models also provide a discrete version of step graphons [11, 26, 39], which are dense in the space of graphons for the topology induced by the cut-norm [39]. Finally, stochastic block models are amenable to a rigorous mathematical analysis, and are indeed at the cutting edge of rigorous probabilistic analysis of random graphs [1].

### 1.8.3 Example of a real-life graph that is well approximated with an SBM

To emphasize the importance of the stochastic block model in the study of real-life graphs, we present a dataset that is studied in detail in Section 6. The data is composed of a time-series of dynamic social-contact graphs collected in a French primary school [71]. The dataset is considered a classic benchmark to study real-life face-to-face contact graphs, and dynamical processes on such graphs (e.g., [4, 13, 14, 20, 25, 31, 41, 42, 43, 67]).

Briefly, students carried RFID tags that recorded (every 20 seconds) face-to-face contacts during two school days [71]. The primary school is composed of ten grades (1-5); each grade is divided into two classes (A & B); each student is a node of the graph. During the school day (8:30 AM – 4:30 PM), events (morning and afternoon recess: 10:30 – 11:00 AM,

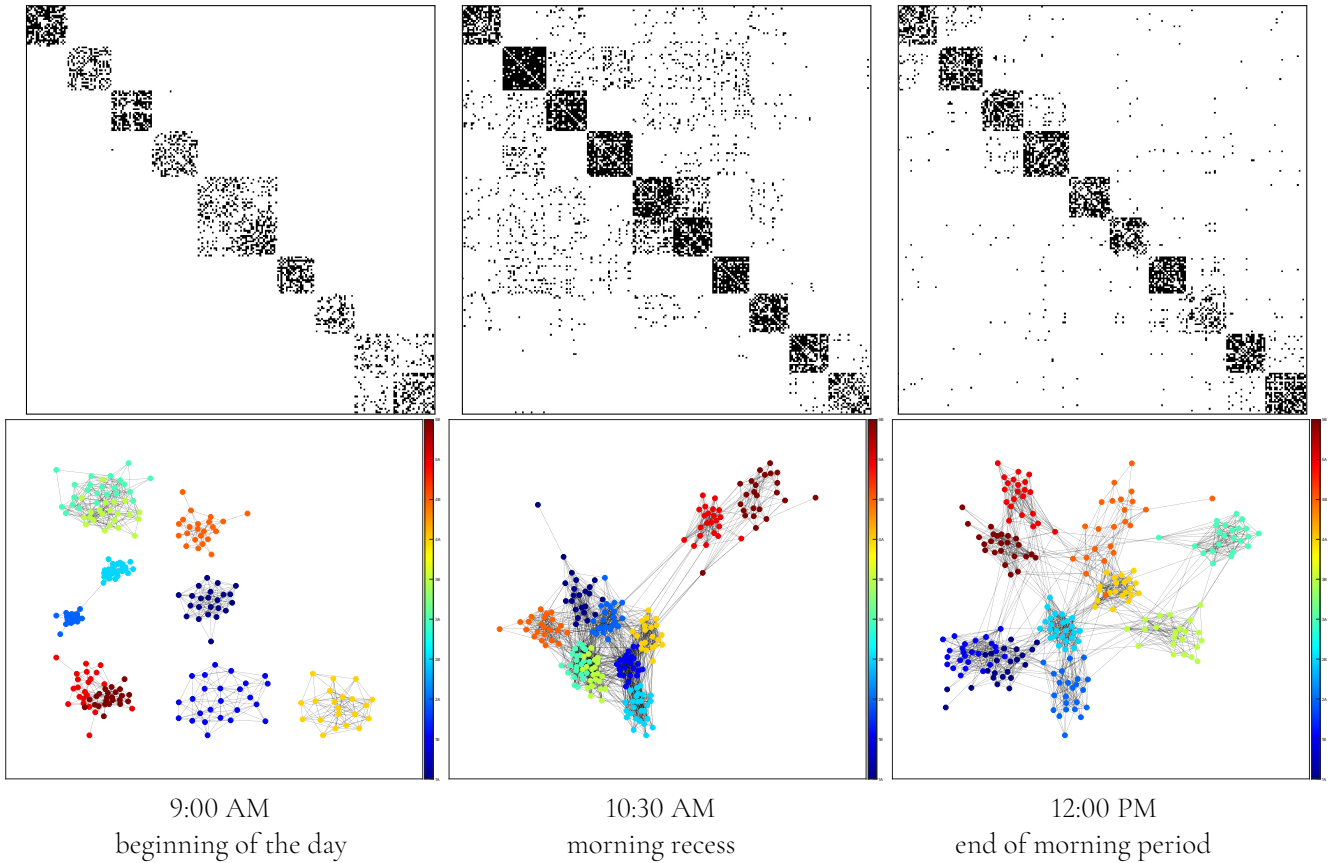


Figure 1: Dynamic face-to-face contact graphs (top: adjacency matrix; bottom: graphical representation). The nodes in the adjacency matrices are grouped from class 1A to class 5B. Each node is a student; the color of the node encodes the class of the student (see colorbar). From left to right: beginning of the school day (9:00 AM); morning recess (10:30 AM), and end of morning period before lunch (12:00 PM).

3:30 – 4:00 PM; lunch periods: 12:00 PM– 1:00 PM, and 1:00 – 2:00 PM) punctuate the school day and trigger significant changes in connectivity and topology of the contact graphs (see Fig. 1).

To facilitate the interpretation of the community structure, we aggregate the graphs over a time window of 40 minutes. The graphs at 9:00 AM (see Fig. 1-left) display the grouping of the two classes of the same grade (second, third, and fifth) caused by a common grade-dependent activity. At 10:30 AM all students mix during recess (see Fig. 1-center). We note that students are preferably in contact with other students from the same grade. A similar connectivity pattern is discernible before the lunch break (see Fig. 1-right).

The graphs displayed in Fig. 1 are examples of real-life graphs that can be well approximated with stochastic block models. Blocks associated with denser connectivity are clearly visible in the adjacency matrices of the graphs at 9:00 AM, 10:30 AM, and 12:00 PM (see top row of Fig. 1). We take note of the merging of the fifth and sixth blocks, and the ninth and tenth blocks, at 9:00 AM. This is also visible in the graphical depiction of the graphs (see left of top and bottom rows of Fig. 1). These contact graphs exhibit intricate dynamics and complex changes in connectivity and structural properties.

A more detailed analysis reveals that the distribution of eigenvalues of the normalized graph Laplacian of these graphs appear similar to the theoretical distributions of the eigenvalues of the normalized graph Laplacian of the stochastic block model (see Fig. 2). Specifically, both distributions reveal the presence of a bump-shaped, centered around 1, which is usually referred as the *bulk*, and which contains most eigenvalues. The presence of the bulk in this dataset is created by the stochastic nature of the graphs. A similar bulk is present in the empirical spectral distribution of the stochastic block model [5, 6, 15, 62, 84]; see also Eq. (16) in Section 2. Starting at 0, there are ten eigenvalues that are separated (this phenomenon is more visually striking in the morning distribution) from the bulk in the morning and afternoon distributions (see left of both distributions in Fig. 2), which is a signature of the stochastic block model.

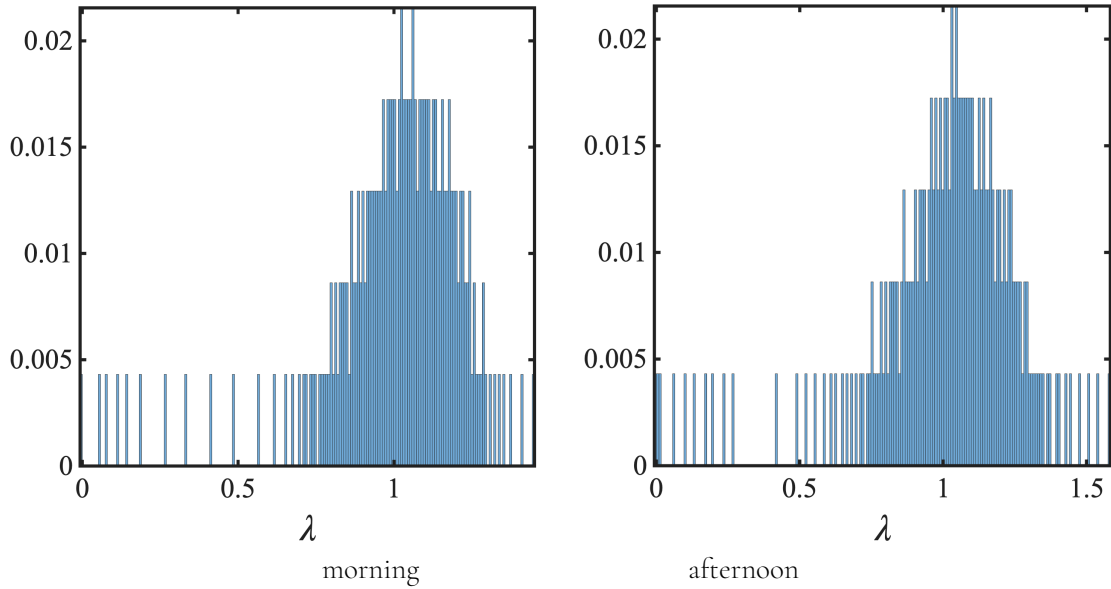


Figure 2: Distribution of the eigenvalues of  $\mathcal{L}$  in the morning (left) and afternoon (right). For both distributions the ten smallest eigenvalues are separated from the bulk.

## 1.9 Content of the paper: overview of the results

The main contribution of this work is a fast algorithm to compute the barycentre of a set of graphs with community structure. The barycentre is determined using a Laplacian spectral pseudo-distance. We solve the problem defined by Eq. (13) by relaxing the optimization problem Eq. (4) and taking

$$\lambda(\widehat{\mu}_T[\mathbb{P}]) = \widehat{\mathbb{E}}_T[\lambda].$$

We then construct  $\Psi$  using the large library of Soules bases [30, 70], which were designed specifically to solve similar inverse eigenvalue problems. This work is significant because it opens the door to the design of new spectral-based graph synthesis [8, 69] that have theoretical guarantees. We publicly share our code to facilitate future work [57].

## 2 A tour of the key ideas

To help guide the intuition of the reader, we highlight the key ideas of our approach. Except for Idea 2, we omit the proofs; Section 4 comprises the rigorous execution of these ideas.

We provide a description of our approach in the most restricted context wherein we can derive proofs for the theorems: the graphs in the sample are random realizations of a balanced stochastic block model,  $\text{SBM}(\mathbf{p}, \mathbf{q}, \mathbf{n})$ . Our experiments (see Section 6) demonstrate that in practice our approach works beyond the controlled environment of balanced stochastic block models; these experiments suggest that our theoretical analysis could be extended to a larger class of community graphs.

**Idea 1.** To solve Eq. (13), we first derive the expression of  $\overline{\mathcal{L}}$  in the case where  $\mathbb{P}$  is a general  $\text{SBM}(\mathbf{p}, \mathbf{q}, \mathbf{n})$ . A simple calculation yields

$$\overline{\mathcal{L}}_{ij} = \begin{cases} -\frac{p_m}{\overline{d}_m} & \text{if } (i, j) \in B_m \times B_m, \\ 1 & \text{if } i = j, \\ -\frac{q}{\sqrt{\overline{d}_m \overline{d}_{m'}}} & \text{if } (i, j) \in B_m \times B_{m'}, m \neq m', \end{cases} \quad (14)$$

where  $\bar{\mathbf{d}}_m \stackrel{\text{def}}{=} \mathbb{E}[\mathbf{d}_{ii}] = |\mathbf{B}_m| \{ \mathbf{p}_m + (\mathbf{n}/|\mathbf{B}_m| - 1)\mathbf{q} \}$  for all nodes  $\mathbf{i} \in \mathbf{B}_m$ .

**Idea 2.** In the case where  $\mathbb{P}$  is a general SBM  $(\mathbf{p}, \mathbf{q}, \mathbf{n})$ , the first  $M$  eigenvalues of  $\mathcal{L}$ ,  $0 = \lambda_1 \leq \dots \leq \lambda_M$  converge to deterministic values as the size of the graph goes to infinity [5, 6, 15, 32, 54, 55, 66, 73]. We propose simplifying Eq. (13) by substituting  $\widehat{\mathbb{E}}_{\mathbf{T}}[\lambda_k]$  for the large graph size deterministic limits.

Unfortunately, closed form expressions of these limits can only be derived for balanced SBM  $(\mathbf{p}, \mathbf{q}, \mathbf{n})$  composed of  $M$  blocks [32, 54, 66]. For this reason, hereafter we assume that  $\mathbb{P} = \text{SBM}(\mathbf{p}, \mathbf{q}, \mathbf{n})$ . In [54], the authors provide the following estimates of the eigenvalues  $\boldsymbol{\lambda}(\mathcal{L})$  of the normalized Laplacian.

**Lemma 1** (Proposition 4.3 of [54]). *Let  $\mathbf{A}$  be a random realization of SBM  $(\mathbf{p}, \mathbf{q}, \mathbf{n})$ , with normalized Laplacian matrix  $\mathcal{L}$ . Then the eigenvalues of  $\mathcal{L}$  are given by*

$$\lambda_m = \mathbf{l}_m + \mathcal{O}\left(\sqrt{\frac{\log \mathbf{n}}{\mathbf{n}}}\right), \quad (15)$$

asymptotically almost-surely, where

$$\mathbf{l}_m = \begin{cases} 0 & \text{if } m = 1, \\ \frac{M\mathbf{q}}{\mathbf{p} + (M-1)\mathbf{q}} & \text{if } 2 \leq m \leq M, \\ 1 & \text{if } M+1 \leq m \leq \mathbf{n}. \end{cases} \quad (16)$$

This result informs the role of the sample eigenvalues  $\widehat{\mathbb{E}}_{\mathbf{T}}[\lambda_m]$ . We expect that only the lowest  $M$  eigenvalues of  $\mathcal{L}$  contribute to the recovery of the geometry and the edge density of SBM  $(\mathbf{p}, \mathbf{q}, \mathbf{n})$ . Conversely, we anticipate that the largest  $\widehat{\mathbb{E}}_{\mathbf{T}}[\lambda_m]$ ,  $M+1 \leq m \leq \mathbf{n}$ , which are created by the stochastic nature of the model and appear in the bulk, [6, 15, 16, 52, 84], do not serve a useful purpose and only contaminate the reconstruction of  $\mathcal{L}(\widehat{\boldsymbol{\mu}}_{\mathbf{T}}[\mathbb{P}])$  in Eq. (5).

To alleviate this issue, we propose to replace the  $\mathbf{n} - M$  largest sample eigenvalues  $\widehat{\mathbb{E}}_{\mathbf{T}}[\lambda_m]$  with their limits  $\mathbf{l}_m$ , and define a “regularized” set of eigenvalues as follows,

$$\widehat{\lambda}_m = \begin{cases} \widehat{\mathbb{E}}_{\mathbf{T}}[\lambda_m] & \text{if } 1 \leq m \leq M, \\ \mathbf{l}_m & \text{if } M+1 \leq m \leq \mathbf{n}. \end{cases} \quad (17)$$

In practice, one needs to estimate  $M$ , the number of eigenvalues outside the bulk. Fortunately, many estimators are available (e.g., [21, 33, 80], and references therein). We use the regularized eigenvalues  $\{\widehat{\lambda}_m\}$  to devise the following estimator of  $\mathcal{L}(\widehat{\boldsymbol{\mu}}_{\mathbf{T}}[\mathbb{P}])$ ,

$$\widehat{\mathcal{L}}_M(\widehat{\boldsymbol{\mu}}_{\mathbf{T}}[\mathbb{P}]) \stackrel{\text{def}}{=} \sum_{k=1}^{\mathbf{n}} \widehat{\lambda}_k \boldsymbol{\psi}_k \boldsymbol{\psi}_k^{\mathbf{T}} = \sum_{k=1}^M \widehat{\mathbb{E}}_{\mathbf{T}}[\lambda_k] \boldsymbol{\psi}_k \boldsymbol{\psi}_k^{\mathbf{T}} + \sum_{k=M+1}^{\mathbf{n}} \mathbf{l}_k \boldsymbol{\psi}_k \boldsymbol{\psi}_k^{\mathbf{T}}. \quad (18)$$

The following lemma provides sufficient conditions for  $\widehat{\mathcal{L}}_M(\widehat{\boldsymbol{\mu}}_{\mathbf{T}}[\mathbb{P}])$  to converge (in the limit of large graph size,  $\mathbf{n} \rightarrow +\infty$ ) toward  $\overline{\mathcal{L}}$  with high probability.

**Lemma 2.** *If the eigenvectors  $\boldsymbol{\Psi} = [\boldsymbol{\psi}_1 \ \dots \ \boldsymbol{\psi}_{\mathbf{n}}]$  satisfy*

$$\begin{cases} \boldsymbol{\psi}_1 = \mathbf{n}^{-1/2} \mathbf{1}, \\ \sum_{k=1}^M \boldsymbol{\psi}_k \boldsymbol{\psi}_k^{\mathbf{T}}(i, j) = \begin{cases} M/\mathbf{n} & \text{if } \exists m \in [M], (i, j) \in \mathbf{B}_m \times \mathbf{B}_m, \\ 0 & \text{otherwise,} \end{cases} \\ \sum_{k=1}^{\mathbf{n}} \boldsymbol{\psi}_k \boldsymbol{\psi}_k^{\mathbf{T}} = \text{Id}, \end{cases} \quad (19)$$

then we have

$$\|\widehat{\mathcal{L}}_M(\widehat{\boldsymbol{\mu}}_T[\mathbb{P}]) - \overline{\mathcal{L}}\|_F = o(1), \quad (20)$$

with probability converging to 1 as the graph size  $\mathbf{n} \rightarrow +\infty$ . In other words, if we replace the sample eigenvalues  $\widehat{\mathbb{E}}_T[\boldsymbol{\lambda}_m]$  with the “regularized” eigenvalues  $\widehat{\boldsymbol{\lambda}}_m$  (defined by Eq. (17)), then the matrix  $\widehat{\boldsymbol{\mu}}_T[\mathbb{P}]$  corresponding to  $\widehat{\mathcal{L}}_M(\widehat{\boldsymbol{\mu}}_T[\mathbb{P}])$  satisfies Eq. (13).

*Proof.* We first specialize Eq. (14) for SBM  $(\mathbf{p}, \mathbf{q}, \mathbf{n})$ , to get

$$\overline{\mathcal{L}} = \text{Id} - \frac{M}{\mathbf{n}(\mathbf{p} + (\mathbf{M} - 1)\mathbf{q})} \mathbf{P}, \quad (21)$$

where  $\mathbf{P}$  is defined in Eq. (11). We then substitute in Eq. (18)  $\widehat{\mathbb{E}}_T[\boldsymbol{\lambda}_m]$ ,  $1 \leq m \leq M$  for the large graph size estimate given by Eq. (16). We obtain with probability converging to 1 as the graph size  $\mathbf{n} \rightarrow +\infty$ ,

$$\widehat{\mathcal{L}}_M(\widehat{\boldsymbol{\mu}}_T[\mathbb{P}]) = \sum_{k=1}^{\mathbf{n}} l_k \boldsymbol{\psi}_k \boldsymbol{\psi}_k^T + \boldsymbol{\varepsilon}_n, \quad (22)$$

where  $\boldsymbol{\varepsilon}_n = o\left(\sqrt{\frac{\log \mathbf{n}}{\mathbf{n}}}\right) \left\{ \sum_{k=1}^M \boldsymbol{\psi}_k \boldsymbol{\psi}_k^T \right\}$ .

Now,

$$\begin{aligned} \sum_{k=1}^{\mathbf{n}} l_k \boldsymbol{\psi}_k \boldsymbol{\psi}_k^T &= \frac{M\mathbf{q}}{\mathbf{p} + (\mathbf{M} - 1)\mathbf{q}} \sum_{k=2}^M \boldsymbol{\psi}_k \boldsymbol{\psi}_k^T + \sum_{k=M+1}^{\mathbf{n}} \boldsymbol{\psi}_k \boldsymbol{\psi}_k^T \\ &= \frac{M\mathbf{q}}{\mathbf{p} + (\mathbf{M} - 1)\mathbf{q}} \sum_{k=1}^M \boldsymbol{\psi}_k \boldsymbol{\psi}_k^T - \frac{M\mathbf{q}}{\mathbf{p} + (\mathbf{M} - 1)\mathbf{q}} \boldsymbol{\psi}_1 \boldsymbol{\psi}_1^T - \sum_{k=1}^M \boldsymbol{\psi}_k \boldsymbol{\psi}_k^T + \sum_{k=1}^{\mathbf{n}} \boldsymbol{\psi}_k \boldsymbol{\psi}_k^T. \end{aligned} \quad (23)$$

Whence

$$\widehat{\mathcal{L}}_M(\widehat{\boldsymbol{\mu}}_T[\mathbb{P}]) = \sum_{k=1}^{\mathbf{n}} \boldsymbol{\psi}_k \boldsymbol{\psi}_k^T - \left\{ \frac{\mathbf{p} - \mathbf{q}}{\mathbf{p} + (\mathbf{M} - 1)\mathbf{q}} \left( \sum_{k=1}^M \boldsymbol{\psi}_k \boldsymbol{\psi}_k^T \right) + \frac{M\mathbf{q}}{\mathbf{p} + (\mathbf{M} - 1)\mathbf{q}} \boldsymbol{\psi}_1 \boldsymbol{\psi}_1^T \right\} + \boldsymbol{\varepsilon}_n, \quad (24)$$

with high probability. If the eigenvectors  $\boldsymbol{\Psi} = [\boldsymbol{\psi}_1 \cdots \boldsymbol{\psi}_n]$  satisfy Eq. (19) then a simple calculation shows that

$$\widehat{\mathcal{L}}_M(\widehat{\boldsymbol{\mu}}_T[\mathbb{P}]) - \overline{\mathcal{L}} = \boldsymbol{\varepsilon}_n, \quad (25)$$

with probability converging to 1 as the graph size  $\mathbf{n} \rightarrow +\infty$ . Finally, since  $\boldsymbol{\Psi}$  is an orthonormal basis, we get

$$\|\boldsymbol{\varepsilon}_n\|_F = o\left(\sqrt{\frac{\log \mathbf{n}}{\mathbf{n}}}\right) \left\| \sum_{k=1}^M \boldsymbol{\psi}_k \boldsymbol{\psi}_k^T \right\|_F = o\left(\sqrt{\frac{\log \mathbf{n}}{\mathbf{n}}}\right) \sqrt{M}. \quad (26)$$

We conclude that  $\|\widehat{\mathcal{L}}_M(\widehat{\boldsymbol{\mu}}_T[\mathbb{P}]) - \overline{\mathcal{L}}\|_F = o(1)$ , with probability converging to 1 as the graph size  $\mathbf{n} \rightarrow +\infty$ .  $\square$

**Idea 3.** Given a sample mean estimate  $\widehat{\mathbb{E}}_T[\mathbb{P}]$  of  $\mathbb{E}[\mathbb{P}]$ , we design an algorithm that explores the library of Soules bases (which is organized as a binary tree [29]), and returns an orthonormal Soules basis  $\boldsymbol{\Psi} = [\boldsymbol{\psi}_1 \cdots \boldsymbol{\psi}_n]$ , that satisfies Eq. (19)

We briefly describe the ideas behind the construction of the sequence of  $\boldsymbol{\psi}_k$  in the library of Soules basis. Because the support of  $\sum_{k=1}^M \boldsymbol{\psi}_k \boldsymbol{\psi}_k^T$  is formed by the  $M$  blocks of the SBM  $(\mathbf{p}, \mathbf{q}, \mathbf{n})$  (see the second condition in Eq. (19)), we design  $\boldsymbol{\psi}_2, \boldsymbol{\psi}_3, \dots, \boldsymbol{\psi}_M$  so that they are constant on each block  $\mathbf{B}_m$ ; and the zero-crossing of  $\boldsymbol{\psi}_k$  is aligned with the jumps between the blocks in  $\widehat{\mathbb{E}}_T[\mathbb{P}]$ .

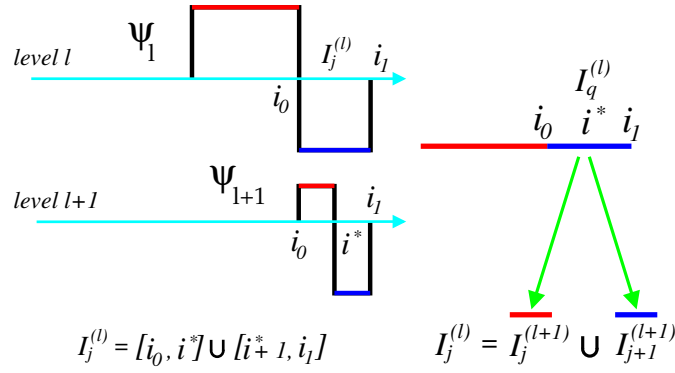


Figure 3: Left:  $\boldsymbol{\psi}_{l+1}$  is created by splitting the block of indices  $I_q^{(l)} = [i_0, i_1]$  at level  $l$  into two sub-blocks,  $[i_0, i^*] \cup [i^* + 1, i_1]$  at level  $l + 1$ . Right: a node in the Soules binary tree is triggered by the splitting of  $[i_0, i_1] = [i_0, i^*] \cup [i^* + 1, i_1]$ .

The construction of the Soules vectors starts at the coarsest scale with  $\boldsymbol{\psi}_1 = \sqrt{n}\mathbf{1}$ . The next Soules vector,  $\boldsymbol{\psi}_2$ , is designed to detect the largest gradient between any pair of blocks  $\mathbf{B}_m \times \mathbf{B}_m$  and  $\mathbf{B}_{m'} \times \mathbf{B}_{m'}$ . In terms of  $\widehat{\mathbb{E}}_{\mathbb{T}}[\mathbb{P}]$ , the zero-crossing of  $\boldsymbol{\psi}_2$  is carefully aligned with the boundaries between two blocks of  $\widehat{\mathbb{E}}_{\mathbb{T}}[\mathbb{P}]$  associated with the largest jump in the edge probability. Whence we can choose  $\boldsymbol{\psi}_2$  to maximize  $|\langle \boldsymbol{\psi}_2 \boldsymbol{\psi}_2^T, \widehat{\mathbb{E}}_{\mathbb{T}}[\mathbb{P}] \rangle|^2$ . The construction of the remaining  $\boldsymbol{\psi}_k$  proceeds iteratively by detecting all the boundaries between the blocks  $\mathbf{B}_m \times \mathbf{B}_m$ . An added benefit of working with Soules bases is that the condition  $\sum_{k=1}^n \boldsymbol{\psi}_k \boldsymbol{\psi}_k^T = \text{Id}$  comes for free [29].

## 2.1 Organization of the paper

For the sake of completeness, we review in Section 3 the concept of Soules bases and their key theoretical properties. The reader who is already familiar with Soules bases can skip to Section 4 wherein we describe the algorithm that computes the Soules basis solution to Eq. (19). The theoretical properties of Algorithm 1 is presented in Section 5. Finally, we report results of experiments on synthetic and real-life datasets in Section 6. In Section 7, we discuss the implications of our work. The proofs of some technical lemmata are left aside in Section 8.

## 3 Soules Bases: definition and properties

Soules bases [29, 70] were invented to provide a solution to the following symmetric nonnegative inverse eigenvalue problem: find  $\boldsymbol{\Psi} \in O(n)$  such that  $\boldsymbol{\Psi} \text{diag}(\lambda_1, \dots, \lambda_n) \boldsymbol{\Psi}^T \in \mathcal{S}$ . Soules bases provide a large family of solutions to this problem.

### 3.1 Definition of Soules Bases

A Soules bases is an orthogonal matrix that is constructed iteratively by applying a product of Givens rotations to a fixed vector  $\boldsymbol{\psi}_1$  with nonnegative entries. The construction starts at the coarsest level ( $l = 1$ ) with a normalized vector  $\boldsymbol{\psi}_1$  with nonnegative entries, whose support is the interval  $I^{(1)} = [n]$ . Hereunder, our analysis assumes that we always choose  $\boldsymbol{\psi}_1 \stackrel{\text{def}}{=} n^{-1/2}\mathbf{1}$ .

At any given level  $l$ , the set  $[n]$  is partitioned into  $l$  ordered intervals  $I_q^{(l)}$ ,  $1 \leq q \leq l$ . When progressing from level  $l$  to  $l + 1$ , one chooses an interval,  $I_q^{(l)} = [i_0, i_1]$ , and one chooses an index  $i^* \in [i_0, i_1]$  and defines  $I_q^{(l+1)} \stackrel{\text{def}}{=} [i_0, i^*]$ , and  $I_{q+1}^{(l+1)} \stackrel{\text{def}}{=} [i^* + 1, i_1]$  (see Fig. 3-right). The split of  $I_q^{(l)}$  into  $I_q^{(l+1)}$  and  $I_{q+1}^{(l+1)}$  triggers the construction of the

Soules vector  $\boldsymbol{\psi}_{\mathbf{i}+1}$  (see Fig. 3-left), defined by

$$\boldsymbol{\psi}_{\mathbf{i}+1}(\mathbf{i}) \stackrel{\text{def}}{=} \frac{1}{\|\boldsymbol{\psi}(\mathbf{i}_0 : \mathbf{i}_1)\|} \begin{cases} \frac{\|\boldsymbol{\psi}_1(\mathbf{i}^* + 1 : \mathbf{i}_1)\|}{\|\boldsymbol{\psi}_1(\mathbf{i}_0 : \mathbf{i}^*)\|} \boldsymbol{\psi}_1(\mathbf{i}) & \text{if } \mathbf{i}_0 \leq \mathbf{i} \leq \mathbf{i}^*, \\ -\frac{\|\boldsymbol{\psi}_1(\mathbf{i}_0 : \mathbf{i}^*)\|}{\|\boldsymbol{\psi}_1(\mathbf{i}^* + 1 : \mathbf{i}_1)\|} \boldsymbol{\psi}_1(\mathbf{i}) & \text{if } \mathbf{i}^* + 1 \leq \mathbf{i} \leq \mathbf{i}_1, \\ 0 & \text{otherwise,} \end{cases} \quad (27)$$

where the vectors  $\boldsymbol{\psi}_1(\mathbf{i}_0 : \mathbf{i}_1)$ ,  $\boldsymbol{\psi}_1(\mathbf{i}_0 : \mathbf{i}^*)$ , and  $\boldsymbol{\psi}_1(\mathbf{i}^* + 1 : \mathbf{i}_1)$  are  $\mathbf{n}$ -dimensional vectors whose nonzero entries are extracted from  $\boldsymbol{\psi}_1$  at the corresponding indices,

$$\begin{aligned} \boldsymbol{\psi}_1(\mathbf{i}_0 : \mathbf{i}_1) &= [0 \cdots 0 \ \boldsymbol{\psi}_1(\mathbf{i}_0) \cdots \boldsymbol{\psi}_1(\mathbf{i}^*) \ \boldsymbol{\psi}_1(\mathbf{i}^* + 1) \cdots \boldsymbol{\psi}_1(\mathbf{i}_1) \ 0 \cdots 0]^\top, \\ \boldsymbol{\psi}_1(\mathbf{i}_0 : \mathbf{i}^*) &= [0 \cdots 0 \ \boldsymbol{\psi}_1(\mathbf{i}_0) \cdots \boldsymbol{\psi}_1(\mathbf{i}^*) \ 0 \cdots 0]^\top, \\ \boldsymbol{\psi}_1(\mathbf{i}^* + 1 : \mathbf{i}_1) &= [0 \cdots 0 \ \boldsymbol{\psi}_1(\mathbf{i}^* + 1) \cdots \boldsymbol{\psi}_1(\mathbf{i}_1) \ 0 \cdots 0]^\top. \end{aligned} \quad (28)$$

The iterative subdivision process can be described using a binary tree (see Fig. 4-right) where a new vector is created at each node that has two children. We observe that  $\boldsymbol{\psi}_k$  and  $\boldsymbol{\psi}_{k'}$ ,  $k \neq k'$ , are either nested, or they do not overlap; whence  $\langle \boldsymbol{\psi}_k, \boldsymbol{\psi}_{k'} \rangle = 0$ , and  $[\boldsymbol{\psi}_1 \cdots \boldsymbol{\psi}_n]$  is an orthonormal matrix [29]; see [75] for a similar construction of Walsh-Hadamard packets and [18] for an analogous construction of complex-valued packets.

### 3.2 Properties of Soules Bases

Using Eq. (27), we derive the following lemma with a proof by induction.

**Lemma 3** (See [29]). *Let  $[\boldsymbol{\psi}_1 \cdots \boldsymbol{\psi}_n]$  be a Soules basis constructed according to Eq. (27). Then,*

$$\forall \mathbf{m} = 1, \dots, \mathbf{n}, \quad \sum_{k=1}^{\mathbf{m}} \boldsymbol{\psi}_k \boldsymbol{\psi}_k^\top \geq 0, \quad \text{and} \quad \sum_{k=1}^{\mathbf{n}} \boldsymbol{\psi}_k \boldsymbol{\psi}_k^\top = \text{Id}. \quad (29)$$

Finally, we have the fundamental property of Soules bases.

**Lemma 4** (See [29]). *Let  $\boldsymbol{\Psi}$  be a Soules basis constructed according to Eq. (27). Let  $\boldsymbol{\Lambda} = \text{diag}(\lambda_1, \dots, \lambda_n)$ , where  $\lambda_1 \geq \lambda_2 \geq \dots \geq \lambda_n$ . Then, the off-diagonal entries of  $\boldsymbol{\Psi} \boldsymbol{\Lambda} \boldsymbol{\Psi}^\top$  are non-negative. In addition, if  $\lambda_n \geq 0$ , then  $\boldsymbol{\Psi} \boldsymbol{\Lambda} \boldsymbol{\Psi}^\top \geq 0$ .*

We note that there has been some recent interest in Soules bases to solve various inverse eigenvalue problems [24, 65].

**Remark 1.** *The result in Lemma 4 relies on the fact that the sequence of eigenvalues is decreasing. On the other hand, the eigenvalues of  $\mathcal{L}$  are by nature ranked in ascending order (the index  $\mathbf{k}$  of eigenvalue  $\lambda_{\mathbf{k}}$  of  $\mathcal{L}$  encodes the frequency of the corresponding eigenvector). Given an ascending sequence of eigenvalues of  $\mathcal{L}$ ,  $0 = \lambda_1 < \lambda_2 \leq \dots \leq \lambda_n$ , we would like to apply Lemma 4 to reconstruct a Laplacian matrix using a Soules basis. Since the off-diagonal entries of a normalized Laplacian  $\mathcal{L}$  are nonpositive, we need to work with  $-\boldsymbol{\lambda}$ . Then,  $0 = \lambda_1 > -\lambda_2 \geq \dots \geq -\lambda_n$ , and we can use Lemma 4 to construct  $\mathcal{L}^*$  such that*

$$\mathcal{L}^* = \boldsymbol{\Psi} \text{diag}(\lambda_1, \dots, \lambda_n) \boldsymbol{\Psi}^\top, \quad \text{where } \mathcal{L}_{ij}^* \leq 0 \text{ if } \mathbf{i} \neq \mathbf{j}. \quad (30)$$

Since we choose,  $\boldsymbol{\psi}_1 = \mathbf{n}^{-1/2} \mathbf{1}$ , we have  $\mathcal{L}^* \mathbf{1} = \mathbf{0}$ , and therefore  $\mathcal{L}_{ii}^* \geq 0$ . While the signs of the entries of  $\mathcal{L}^*$  match those of a normalized Laplacian, there is no guarantee that  $\mathcal{L}^*$  be a valid normalized Laplacian (but see a definite answer in the case of the combinatorial Laplacian,  $\mathbf{L} = \mathbf{D} - \mathbf{A}$  in [24]).

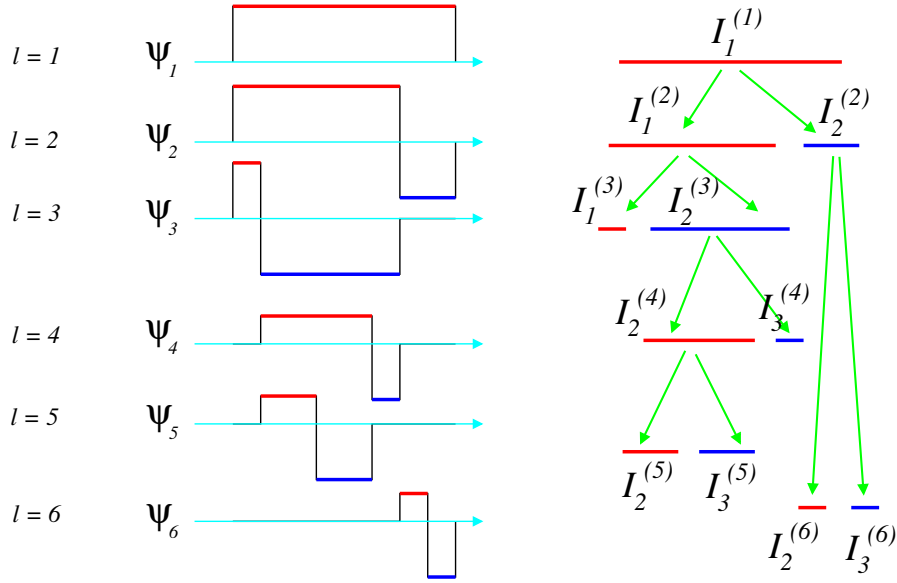


Figure 4: Left: starting from level  $l = 1$ , one Soules vector  $\psi_l$  is constructed at each level  $l \geq 2$  by selecting and then splitting an interval  $I_j^{(l)}$  over which  $\forall l \leq k \leq l$ ,  $\psi_k|_{I_j^{(l)}}$  is constant. Right: each Soules basis is associated with a binary tree. The leaves of the tree are intervals that are not split.

## 4 A Soules Basis solution to Eq. (19)

### 4.1 A greedy exploration of the Soules library

Given  $T$  independent realizations of SBM  $(p, q, n)$ , represented by their adjacency matrices  $\mathbf{A}^{(1)}, \dots, \mathbf{A}^{(T)}$ , we describe in this section a greedy algorithm that constructs a Soules basis  $[\psi_1 \cdots \psi_n]$  that solves Eq. (19).

As explained in Section 2 (Idea 3), the construction of the Soules vectors proceeds using a multiscale approach. One starts at the coarsest scale with  $\psi_1 = n^{-1/2}\mathbf{1}$ . The next vector,  $\psi_2$ , is chosen so that it detects the two communities with the largest difference in edge probability. In terms of the sample adjacency matrix, the zero-crossing of  $\psi_2$  is aligned with the boundaries between two blocks of  $\widehat{\mathbf{E}}_T[\mathbb{P}]$  associated with the largest jump in the edge probability.

Wherefore we choose  $\psi_2$  to maximize  $|\langle \psi_2 \psi_2^T, \widehat{\mathbf{E}}_T[\mathbb{P}] \rangle|^2$ . The next Soules vector,  $\psi_3$ , has its support inside either one of the two sets  $\{\psi_2 \geq 0\}$  or  $\{\psi_2 \leq 0\}$ . We can therefore detect the second largest jump in the edge probability by maximizing the magnitude of the inner product between  $\psi_3 \psi_3^T$  and the reconstruction error,  $[\widehat{\mathbf{E}}_T[\mathbb{P}] - \langle \widehat{\mathbf{E}}_T[\mathbb{P}], \psi_2 \psi_2^T \rangle \psi_2 \psi_2^T]$ ,

$$\begin{aligned} \psi_3 &= \underset{\psi_3 \text{ defined by Eq. (27)}}{\operatorname{argmax}} \left| \langle \psi_3 \psi_3^T, [\widehat{\mathbf{E}}_T[\mathbb{P}] - \langle \widehat{\mathbf{E}}_T[\mathbb{P}], \psi_2 \psi_2^T \rangle \psi_2 \psi_2^T] \rangle \right|^2, \\ &= \underset{\psi_3 \text{ defined by Eq. (27)}}{\operatorname{argmax}} \left| \langle \psi_3 \psi_3^T, \widehat{\mathbf{E}}_T[\mathbb{P}] \rangle \right|^2, \end{aligned} \quad (31)$$

since  $\psi_3^T \psi_2 = 0$ . At level  $l$ , the algorithm selects the new Soules vector  $\psi_{l+1}$  that maximizes the magnitude of the inner product between  $\psi_{l+1} \psi_{l+1}^T$  and  $\widehat{\mathbf{E}}_T[\mathbb{P}]$ ,

$$\psi_{l+1} = \underset{\psi_{l+1} \text{ defined by Eq. (27)}}{\operatorname{argmax}} \left| \langle \psi_{l+1} \psi_{l+1}^T, \widehat{\mathbf{E}}_T[\mathbb{P}] \rangle \right|^2. \quad (32)$$

Algorithm 1 provides the pseudocode for the implementation of this algorithm.

---

**Algorithm 1** Top-down exploration of the Soules binary tree.

```

1: procedure BESTSOULESBASIS( $\widehat{\mathbf{E}}_T[\mathbb{P}], \Psi$ )  $\triangleright$  Input:  $\widehat{\mathbf{E}}_T[\mathbb{P}]$ ; Output:  $\Psi$  the Soules matrix
2:    $\psi_1 \leftarrow n^{-1/2}\mathbf{1}$ 
3:   for all levels  $l \in \{1, \dots, n-1\}$  do
4:      $\triangleright$  For each block  $I_q^{(l)} = [i_0, i_1]$  which was not split at level  $l$  we split it using an index  $i^* \in [i_0, i_1]$  and construct the
       eigenvector  $\psi_{l+1}$  associated with the split. We compute  $|\langle \psi_{l+1} \psi_{l+1}^T, \widehat{\mathbf{E}}_T[\mathbb{P}] \rangle|^2$ 
5:      $i^* \leftarrow 1$   $\triangleright$  index of the tentative  $\psi_{l+1}$  at level  $l$ 
6:     for all blocks  $I_q^{(l)}$  at level  $l$  do  $\triangleright$  there are exactly  $l$  blocks at level  $l$ 
7:        $i_0 \leftarrow \text{leftend}(I_q^{(l)}); i_1 \leftarrow \text{rightend}(I_q^{(l)})$   $\triangleright I_q^{(l)} = [i_0, i_1]$ 
8:       if ( $i_0 < i_1$ ) then  $\triangleright$  the block  $I_q^{(l)}$  is not a leaf
9:         for all  $i^* \in \{i_0, \dots, i_1\}$  do
10:           $\psi_{l+1} \leftarrow \text{buildvector}([i_0, i_1], i^*)$   $\triangleright$  construct  $\psi_{l+1}$  using Eq. (27)
11:           $\text{coeff}(i^*) \leftarrow |\langle \psi_{l+1} \psi_{l+1}^T, \widehat{\mathbf{E}}_T[\mathbb{P}] \rangle|^2$ 
12:           $i^* \leftarrow i^* + 1$   $\triangleright$  update the index of the next tentative  $\psi_{l+1}$ 
13:        end for  $\triangleright$  next index  $i^*$  so that  $[i_0, i_1] = [i_0, i^*] \cup [i^* + 1, i_1]$ 
14:      end if
15:    end for  $\triangleright$  move to the next block at level  $l$ 
16:     $\triangleright$  We have explored all the blocks at level  $l$ . We now find the block  $[i_0, i_1]$  and the index  $i^*$  of the split that result in
       the largest  $|\langle \psi_{l+1} \psi_{l+1}^T, \widehat{\mathbf{E}}_T[\mathbb{P}] \rangle|^2$ . We save the corresponding  $\psi_{l+1}$  in  $\Psi$ 
17:     $([i_0, i_1], i^*) \leftarrow \underset{i_0, i_1}{\text{argmax}} \underset{i^* \in \{i_0, \dots, i_1\}}{\text{argmax}} (\text{coeff})$ 
18:     $I_q^{(l+1)} \leftarrow [i_0, i^*]; I_{q+1}^{(l+1)} \leftarrow [i^* + 1, i_1]$ 
19:     $\psi_{l+1} \leftarrow \text{buildvector}(I_q^{(l+1)}, I_{q+1}^{(l+1)})$   $\triangleright$  use Eq. (27) to construct  $\psi_{l+1}$ 
20:     $\Psi(:, l+1) \leftarrow \psi_{l+1}$   $\triangleright$  add  $\psi_{l+1}$  to the Soules basis
21:  end for  $\triangleright$  go down to a finer level
22:  return  $\Psi$   $\triangleright$  return the Soules basis
23: end procedure

```

---

## 4.2 Spectral clustering of the nodes.

The greedy construction of the Soules basis necessitates that  $\widehat{\mathbf{E}}_T[\mathbb{P}]$  be “well-aligned” – in the sense that nodes are aggregated in clusters wherein the local node connectivity is approximately constant. This required step is equivalent to the estimation of a piecewise constant graphon for each observed graph in [49]. We use a spectral clustering method based on the eigenvectors of the normalized graph Laplacian [22, 58, 68] to organize nodes into clusters; the algorithm only requires the knowledge of the number  $M$  of clusters. This prerequisite step only provides a grouping of the nodes based on the connectivity measurements (see Fig. 5). After this coarse clustering, the adjacency matrices  $\mathbf{A}^{(1)}, \dots, \mathbf{A}^{(T)}$  are not aligned: one cannot match the nodes from one graph to another. In short, this step corresponds to the approximation of each  $\mathbf{A}^{(t)}$  using a step graphon (e.g., [3, 11, 36, 39, 49, 53, 61, 78]). As demonstrated in the experiments, the clustering of the nodes into communities is not always accurate. Fortunately, the choice of the Soules vectors in Algorithm 1 only relies on the coarse scale eigenvectors. These eigenvectors are determined by computing  $|\langle \psi_l \psi_l^T, \widehat{\mathbf{E}}_T[\mathbb{P}] \rangle|^2$ . The support of  $\psi_k \psi_k^T$  is large for  $k = 2, 3, \dots$ , and  $\psi_k \psi_k^T$  is piecewise constant. The random noise in  $\widehat{\mathbf{E}}_T[\mathbb{P}]$  – created by the incorrect assignment of nodes to the wrong community – is partly suppressed when computing  $|\langle \psi_k \psi_k^T, \widehat{\mathbf{E}}_T[\mathbb{P}] \rangle|^2$ . Fig. 5 demonstrates the coarse clustering (see Fig. 5-right) applied on a randomly permuted adjacency matrix (see Fig. 5-center) of the SBM  $(\mathbf{p}, \mathbf{q}, n)$  model (see Fig. 5-left).

The inherent uncertainty associated with the cluster labels is resolved by ranking the clusters according to their volume. This spectral clustering only requires that we compute the  $M$  dominant eigenvectors of the sample symmetric normalized adjacency matrix,  $\widehat{\mathbf{E}}_T[\widehat{\mathbf{A}}]$ , and therefore does not increase significantly the computational load of the algorithm.

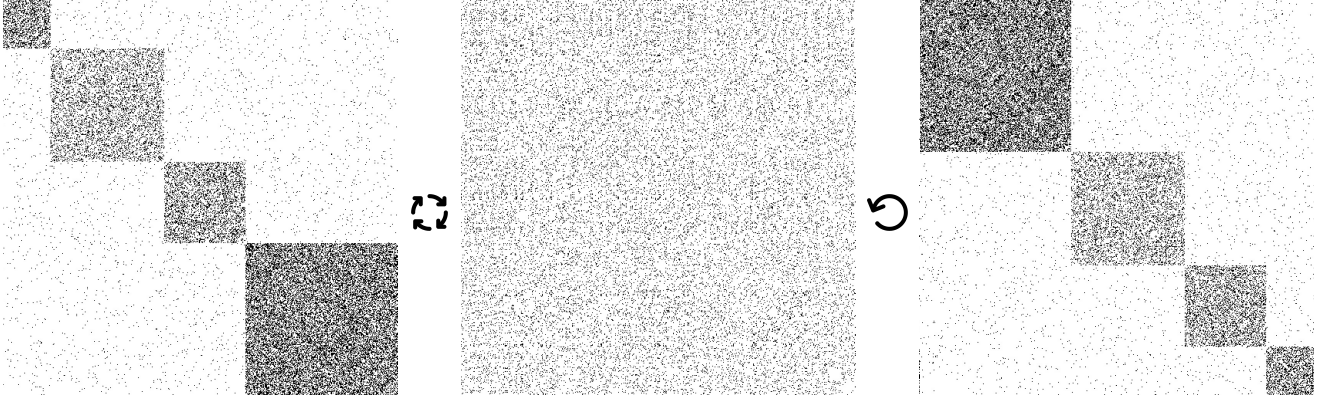


Figure 5: Left: the adjacency matrix of a random realization of the SBM  $(\mathbf{p}, \mathbf{q}, \mathbf{n})$  model. We have  $M = 4$  communities of sizes 63, 147, 105, 197; the graph size is  $\mathbf{n} = 512$ ; the edge probability within community  $\mathbf{i}$  was  $p_{\mathbf{i}} \propto (\log \mathbf{n})^2/\mathbf{n}$ . The edge probability across communities was  $\mathbf{q} = 2(\log \mathbf{n})/\mathbf{n}$ . Center: the adjacency matrix is permuted with a random permutation. Right: coarse clustering of the randomly permuted matrix. This last adjacency matrix is the input to Algorithm 1; see Fig. 6-left.

#### 4.2.1 Algorithmic Complexity

The optimization problem given by Eq. (13) cannot be solved with a brute-force search, since we search  $\Psi$  over the orthogonal group  $O(\mathbf{n})$ . Polynomial-time numerical methods [12] have been devised to take advantage of the lower dimension of this Riemannian submanifold. In comparison, the computational complexity of Algorithm 1 is linear in  $\mathbf{n}$ .

We need to process  $M$  levels; the discovery of  $\psi_{\mathbf{m}}$  at each level  $\mathbf{m}$  requires that we evaluate  $\left| \langle \psi_{\mathbf{m}+1} \psi_{\mathbf{m}+1}^T, \widehat{\mathbb{E}}_{\mathbf{T}}[\mathbb{P}] \rangle \right|^2$   $\mathbf{n}$  times, for an overall complexity of  $M\mathbf{n}$ .

#### 4.3 Theoretical guarantees for the algorithm.

Our analysis of Algorithm 1 is performed under the assumption that the input to the algorithm is not the sample mean adjacency matrix  $\widehat{\mathbb{E}}_{\mathbf{T}}[\mathbb{P}]$  but its population equivalent  $\mathbf{P} = \mathbb{E}[\mathbb{P}]$ . Our experiments (see Fig. 8-left) confirm the validity of this assumption. A finite sample analysis of the error bounds is left for future work. The following lemma proves that the first  $M$  vectors of the Soules basis estimated by Algorithm 1 solve Eq. (19). Unlike Lemma 1, Lemma 5 holds for all SBM, not just balanced SBM.

**Lemma 5.** *Let  $\mathbf{P}$  be the population mean adjacency matrix of SBM  $(\mathbf{p}, \mathbf{q}, \mathbf{n})$  defined by*

$$\mathbf{P} = \sum_{\mathbf{m}=1}^M (p_{\mathbf{m}} - \mathbf{q}) \mathbf{1}_{\mathbf{B}_{\mathbf{m}}} \mathbf{1}_{\mathbf{B}_{\mathbf{m}}}^T + \mathbf{q} \mathbf{J}, \quad (33)$$

where the  $M$  blocks  $\{\mathbf{B}_{\mathbf{m}}\}$  form a partition of  $[\mathbf{n}]$ . Let  $J_{\mathbf{l}}, 1 \leq \mathbf{l} \leq M$  be the leaves in the binary Soules tree (these are the  $M$  intervals that are no longer split, see Fig. 4-right) after  $M$  steps of Algorithm 1. Then, the  $M$  blocks  $\{\mathbf{B}_{\mathbf{m}}\}$  in Eq. (33) coincide with  $M$  the intervals  $\{J_{\mathbf{l}}\}$ . The entries of the matrix  $\sum_{\mathbf{k}=1}^M \psi_{\mathbf{k}} \psi_{\mathbf{k}}^T$  satisfy

$$\sum_{\mathbf{k}=1}^M \psi_{\mathbf{k}} \psi_{\mathbf{k}}^T(\mathbf{i}, \mathbf{j}) = \begin{cases} \frac{1}{|J_{\mathbf{m}}|} & \text{if } (\mathbf{i}, \mathbf{j}) \in J_{\mathbf{m}} \times J_{\mathbf{m}}, \\ 0 & \text{otherwise,} \end{cases} \quad (34)$$

where  $|J_{\mathbf{m}}|$  is the length of the interval  $J_{\mathbf{m}}$ .

The proof of Lemma 5 can be found in Section 8.1. The proof relies on two different facts. The first shows that a top-down exploration of the Soules binary tree, when the first Soules vector is  $\boldsymbol{\psi}_1 = \mathbf{n}^{-1/2}\mathbf{1}$ , always creates a matrix  $\mathbf{E}_M = \sum_{k=1}^M \boldsymbol{\psi}_k \boldsymbol{\psi}_k^\top$  that is piecewise constant on square blocks aligned along the diagonal, and zero outside of the blocks (see Corollary 2). This property only relies on the fact that the sequence of  $\{\boldsymbol{\psi}_k\}_{1 \leq k \leq M}$  have nested supports.

The second result specifically addresses the construction of each  $\boldsymbol{\psi}_k$  in Algorithm 1. We prove in Lemma 9 that at each level  $k$ , the Soules vector  $\boldsymbol{\psi}_k$  returned by Algorithm 1 is aligned with the boundary of a block  $\mathbf{B}_m$  of the edge probability matrix  $\mathbf{P}$ . At level  $M$ , Algorithm 1 has discovered all the  $M$  blocks.

**Corollary 1.** *Let  $\boldsymbol{\Psi} \stackrel{\text{def}}{=} [\boldsymbol{\psi}_1 \cdots \boldsymbol{\psi}_n]$  be the Soules basis returned by Algorithm 1. Then  $\boldsymbol{\Psi}$  solves Eq. (19).*

After Algorithm 1 returns  $[\boldsymbol{\psi}_1 \cdots \boldsymbol{\psi}_n]$  of  $\mathcal{L}(\widehat{\boldsymbol{\mu}}_T[\mathbb{P}])$ , we reconstruct  $\widehat{\boldsymbol{\mu}}_T[\mathbb{P}]$  using Eq. (7).

## 5 The reconstruction of $\widehat{\boldsymbol{\mu}}_T[\mathbb{P}]$

By virtue of being normalized,  $\mathcal{L}$  cannot reveal the corresponding adjacency matrix  $\mathbf{A}$ . Indeed, from Eq. (2), we have

$$\mathbf{A} = \mathbf{D}^{1/2}(\text{Id} - \mathcal{L})\mathbf{D}^{1/2}, \quad (35)$$

and therefore we need the knowledge of the degree matrix  $\mathbf{D}$  to recover  $\mathbf{A}$ . We describe in the next paragraph an estimator  $\widehat{\mathbf{D}}$  of the degree matrix of  $\widehat{\boldsymbol{\mu}}_T[\mathbb{P}]$ .

### 5.1 Estimation of the degree matrix of $\widehat{\boldsymbol{\mu}}_T[\mathbb{P}]$

We observe that Lemma 5 yields an estimate of the location of the blocks  $\mathbf{B}_m \times \mathbf{B}_m$ ,  $1 \leq m \leq M$  associated with SBM  $(\mathbf{p}, \mathbf{q}, \mathbf{n})$ . An estimate of the degree matrix,  $\widehat{\mathbf{D}}$ , is obtained by averaging the degrees of all the nodes in each block  $\mathbf{B}_m$  of  $\widehat{\mathbf{E}}_T[\mathbb{P}]$ ,

$$\widehat{\mathbf{d}}_m \stackrel{\text{def}}{=} \sum_{(i,j) \in \mathbf{B}_m \times \mathbf{B}_m} [\widehat{\mathbf{E}}_T[\mathbb{P}]]_{ij}, \quad 1 \leq m \leq M. \quad (36)$$

A quick calculation confirms that the estimator  $\widehat{\mathbf{d}}_m$  concentrates around the “within block” expected degree  $\bar{\mathbf{d}}_m$  (see Eq. (14)). We have

$$\widehat{\mathbf{d}}_m = T^{-1} \sum_{t=1}^T \sum_{(i,j) \in \mathbf{B}_m \times \mathbf{B}_m} \alpha_{ij}^{(t)}. \quad (37)$$

Therefore  $\widehat{\mathbf{d}}_m$  is the sum of  $T$  independent binomial random variables, and it concentrates around its mean  $\bar{\mathbf{d}}_m$ . The variation of  $\widehat{\mathbf{d}}_m$  around  $\bar{\mathbf{d}}_m$  is bounded by Hoeffding inequality,

$$\forall m \in [M], \forall T \geq 1, \forall \delta > 0, \mathbb{P}\left(\left|\widehat{\mathbf{d}}_m - \bar{\mathbf{d}}_m\right| \geq \delta\right) \leq \exp\left(-4T\delta^2/(|\mathbf{B}_m|(|\mathbf{B}_M| - 1))\right). \quad (38)$$

We recall that  $\bar{\mathbf{d}}_m \stackrel{\text{def}}{=} \mathbb{E}[\mathbf{d}_{ii}] = |\mathbf{B}_m| \{\mathbf{p}_m + (\mathbf{n}/|\mathbf{B}_m| - 1)\mathbf{q}\}$ . Since we always have  $\mathbf{p}_i \gg \mathbf{q}$  (when  $\mathbf{p}_i \approx \mathbf{q}$ , communities can no longer be detected [1, 60]), we can neglect  $\mathbf{q}$  in the estimation of  $\bar{\mathbf{d}}_m$ . Wherefore we conclude that  $\widehat{\mathbf{d}}_m$  is asymptotically unbiased when the sample size  $T \rightarrow +\infty$ .

### 5.2 An estimator of the adjacency matrix of the barycentre graph

We conclude from Eq. (7) that we have

$$\widehat{\boldsymbol{\mu}}_T^M[\mathbb{P}] \stackrel{\text{def}}{=} \widehat{\mathbf{D}}^{1/2}(\text{Id} - \widehat{\mathcal{L}}_M(\widehat{\boldsymbol{\mu}}_T[\mathbb{P}]))\widehat{\mathbf{D}}^{1/2}, \quad (39)$$

where  $\widehat{\mathcal{L}}_M(\widehat{\boldsymbol{\mu}}_T[\mathbb{P}])$  is given by Eq. (18), and  $\widehat{\mathbf{D}}$  is given by Eq. (36).

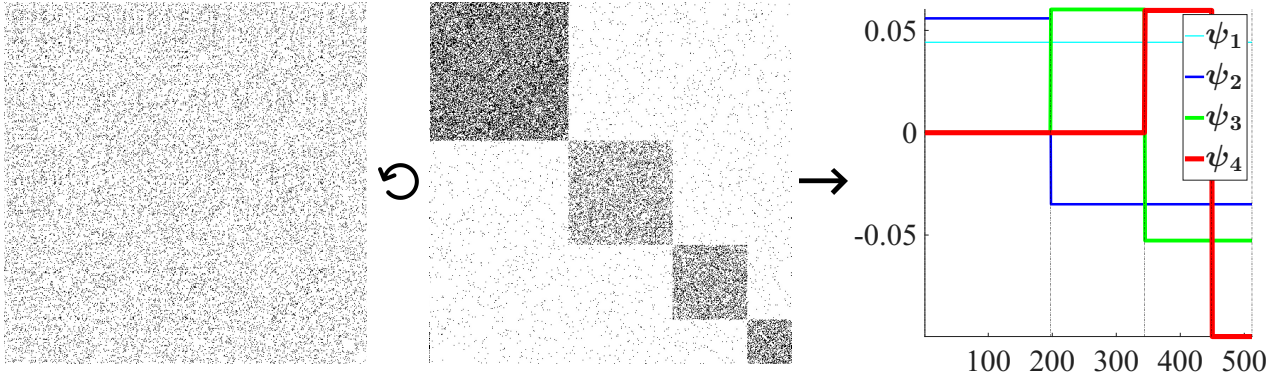


Figure 6: Left: the realization of  $\text{SBM}(\mathbf{p}, \mathbf{q}, \mathbf{n})$  shown in Fig. 5 after a random permutation. Center: coarse clustering of the randomly permuted matrix. After grouping nodes into homogeneous clusters, we have  $M = 4$  communities of sizes 197, 105, 147, 63; the graph size is  $\mathbf{n} = 512$ . The first four trivial Soules vectors accurately detected the boundaries between the blocks (see bars indicating the edge boundaries), in spite of the very low contrast between the communities (see Fig. 5-left).

## 6 Experiments

### 6.1 Random graph models

We compare our theoretical analysis to finite sample estimates, which were computed using numerical simulations. The software used to conduct the experiments is publicly available [57]. All graphs were generated using the  $\text{SBM}(\mathbf{p}, \mathbf{q}, \mathbf{n})$  model. The nodes of the random realizations of the adjacency matrices are permuted with a different random permutation for each realization (e.g., see Fig. 5-centre).

#### 6.1.1 Experimental validation of Lemma 5

The first experiment provides a validation of Lemma 5. For this experiment, we use a regular  $\text{SBM}(\mathbf{p}, \mathbf{q}, \mathbf{n})$  that is not balanced. The number of communities is similar to the numbers that are used in the literature (e.g., [3, 26, 39, 44, 61]). Because the  $\text{SBM}(\mathbf{p}, \mathbf{q}, \mathbf{n})$  is not balanced, we are effectively testing Algorithm 1 outside of the theoretical guarantees provided by Lemma 5.

We use  $M = 4$  communities of sizes 63, 147, 105, 197 (see Fig. 5-left). The edge probabilities were given by  $\mathbf{p}_i = \mathbf{c}_i \log \mathbf{n}^2 / \mathbf{n}$ , where the scaling factor  $\mathbf{c}_i$  was chosen randomly in  $[1, 4]$ , and  $\mathbf{q} = 2 \log \mathbf{n} / \mathbf{n}$ . These edge probabilities yield sparse graphs that are connected almost surely. We generate a randomly permuted single realisation of the  $\text{SBM}(\mathbf{T} = 1)$  (see Fig. 5-centre, and Fig. 6-left).

We first illustrate the selection of the Soules vectors (guaranteed by Lemma 5). The case  $\mathbf{T} = 1$  is the least favorable scenario, since we do not expect that the sample mean adjacency matrix  $\widehat{\mathbb{E}}_{\mathbf{T}}[\mathbb{P}]$  be close to the population mean adjacency matrix  $\mathbb{E}[\mathbb{P}]$ . In addition, all the blocks have different sizes (the  $\text{SBM}$  is not balanced), and the hypotheses of Lemma 5 do not hold. Whence we expect that the estimation of the Soules basis to be most challenging. As shown in Fig. 6-right, the first three non trivial Soules vectors accurately detected the boundaries between the blocks (vertical bars located at  $\mathbf{i} = 63, 210, 315$  mark the block boundaries), in spite of the very low contrast between the communities (see Fig. 5-left). This numerical evidence supports the theoretical analysis of Lemma 5. We then evaluated the accuracy of Eq. (39). Fig. 7-left displays the original edge probability matrix  $\mathbf{P} = \mathbb{E}[\mathbb{P}]$ ; Fig. 7-center displays the adjacency matrix of the barycentre graph  $\widehat{\boldsymbol{\mu}}_{\mathbf{T}}^M[\mathbb{P}]$  using the top  $M = 4$  Soules vectors, and Fig. 7-right displays the residual error  $\mathbb{E}[\mathbb{P}] - \widehat{\boldsymbol{\mu}}_{\mathbf{T}}^M[\mathbb{P}]$ . The mean squared error, defined by

$$\mathbf{n}^{-2} \|\mathbb{E}[\mathbb{P}] - \widehat{\boldsymbol{\mu}}_{\mathbf{T}}^M[\mathbb{P}]\|_{\text{F}}^2 \stackrel{\text{def}}{=} \frac{1}{\mathbf{n}^2} \sum_{i=1}^{\mathbf{n}} \sum_{j=1}^{\mathbf{n}} |p_{ij} - \widehat{p}_{ij}|^2, \quad (40)$$

was  $3.0484e - 05$ .

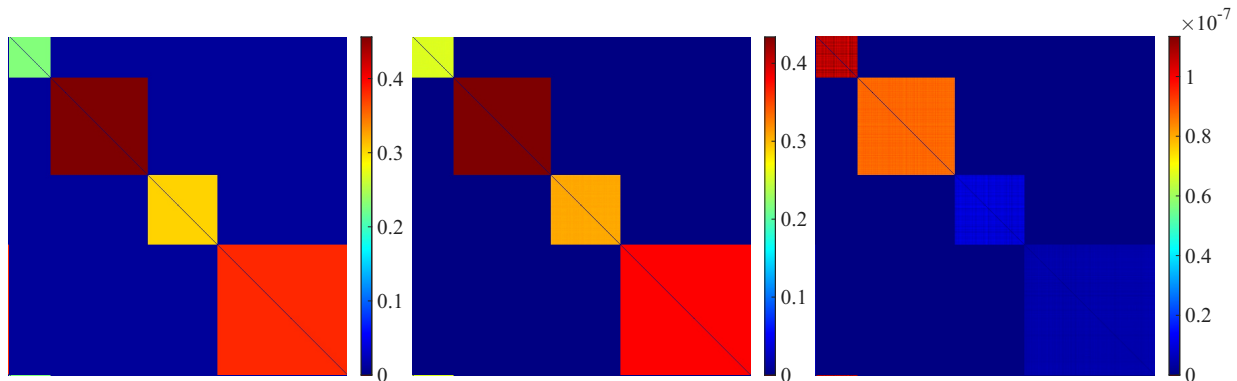


Figure 7: Left: the edge probability matrix  $\mathbb{E}[\mathbb{P}] = \mathbf{P}$  associated with SBM  $(\mathbf{p}, \mathbf{q}, \mathbf{n})$  that was used to generate the adjacency matrix in Fig. 5-left; center: the barycentre graph  $\hat{\mu}_T^M[\mathbb{P}]$ , given by Eq. (39); right: the residual error between  $\mathbf{P}$  and  $\hat{\mu}_T^M[\mathbb{P}]$ .

### 6.1.2 Rate of convergence of $\hat{\mu}_T^M[\mathbb{P}]$ as a function of the graph size

Lemma 2 promises that  $\mathcal{L}(\hat{\mu}_T^M[\mathbb{P}])$  converges to  $\bar{\mathcal{L}}$  with probability converging to 1 as the graph size  $\mathbf{n} \rightarrow +\infty$ . Therefore, we studied the effect of the graph size,  $\mathbf{n}$ , on the mean squared error (see Fig. 8-left). We rescaled the  $M = 4$  SBM  $(\mathbf{p}, \mathbf{q}, \mathbf{n})$  model described in the previous paragraph, keeping the relative sizes of the communities the same, and increased the graph size from  $\mathbf{n} = 100$  to  $\mathbf{n} = 1,075$ . For each value of  $\mathbf{n}$ , we computed the mean squared error (Eq. (40)). As expected, the error decreases as a function of  $\mathbf{n}$ .

We found  $\mathbf{n}^{-2} \|\mathbb{E}[\mathbb{P}] - \hat{\mu}_T^M[\mathbb{P}]\|_F^2 \propto \mathbf{n}^{-1.84}$ . This rate of convergence is of the same order as the optimal (minimax) rate for the estimation of graphons under the mean squared error [39, 61, 79]. Since  $\hat{\mu}_T^M[\mathbb{P}]$  is a stochastic block model we do not expect the underlying graphon to be smooth, and therefore the optimal rate is the bound  $\mathbf{n}^{-1} \log(M) + \mathbf{n}^{-2} M^2$  [39, 61, 79].

We note that the alignment performed by the spectral clustering is not always accurate (as reflected by the presence of outliers in the plot of the mean squared error; e.g.,  $\mathbf{n} = 374$  in Fig. 8-left). This is due to the fact that we use a simple

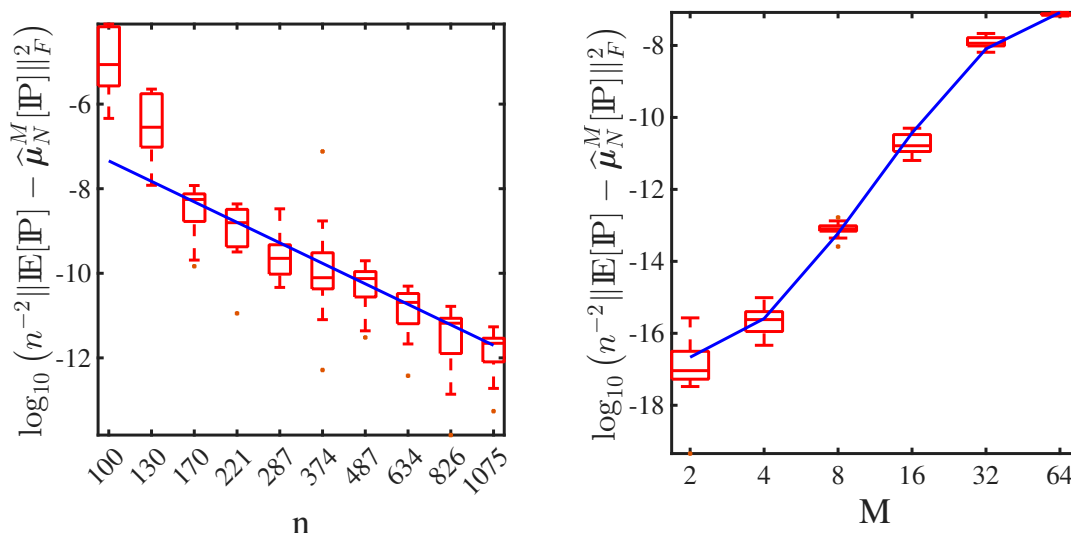


Figure 8: Left: mean squared error  $\mathbf{n}^{-2} \|\mathbb{E}[\mathbb{P}] - \hat{\mu}_T^M[\mathbb{P}]\|_F^2$  as a function of the graph size,  $\mathbf{n}$ . The graph is composed of  $M = 4$  communities, and is a scaled version of the graph shown in Fig. 5-left. Right: mean squared error  $\mathbf{n}^{-2} \|\mathbb{E}[\mathbb{P}] - \hat{\mu}_T^M[\mathbb{P}]\|_F^2$  as a function of the number of blocks,  $M$ . Each graph is sampled from a balanced SBM  $(\mathbf{p}, \mathbf{q}, \mathbf{n})$  with  $M$  blocks of size  $\mathbf{n}/M$ ;  $\mathbf{p}_i = 3(\log \mathbf{n})^2/\mathbf{n}$ ,  $\mathbf{q} = 2 \log \mathbf{n}/\mathbf{n}$ , and  $\mathbf{n} = 1,024$ .

spectral clustering algorithm. The present work focuses on the construction of the barycentre graph; the study of the combined performance of the pre-processing step with the computation of the barycentre is left for future work.

### 6.1.3 Effect of the number of blocks $M$

The next experiment illustrates the effect of the number of blocks  $M$  in a balanced SBM  $(\mathbf{p}, \mathbf{q}, \mathbf{n})$  when the edge probabilities are equal,  $\mathbf{p}_1 = \dots = \mathbf{p}_M$ . When  $M$  becomes large, then the first  $M - 1$  non trivial eigenvalues  $\lambda_m$  of  $\mathcal{L}$ , converge to 1. Because these eigenvalues are no longer separated from the bulk, the regularized reconstruction Eq. (18) becomes numerically unstable, and the reconstruction error increases (see Fig. 8-right).

## 6.2 Real world graphs

We evaluated the performance of our algorithm on a time-sequence of social-contact graphs, collected via RFID tags in an French primary school [71]. The dataset was described earlier in Section 1.8. In this dataset, the time-varying graphs undergo significant structural changes as they evolve in time (e.g., merging of two classes, or the emergence of a single subgraph as a connective hub between disparate regions of the graph (see Fig. 9).

This dataset has been used as a standard benchmark to quantify the performance of sophisticated algorithms to analyse dynamic networks, which exhibit intricate dynamics and complex changes in connectivity and structural properties [14, 25, 31, 4, 41, 67]. For the purpose of this experiment, we think of each class as a community of connected students; despite the fact that classes are weakly connected (e.g., see Fig. 9 at times 9:00 a.m., and 2:03 p.m.), the goal of the experiment is to recover the communities determined by the classes using the subset of graphs associated with the morning and afternoon periods separately. We divide the school day into morning (8:30 AM–12:00 PM) and afternoon (2:00 PM–4:30 PM). We exclude the lunch period because many students leave the school to take their lunch at home. The morning period is divided into  $T = 35$  time intervals of approximately 6 minutes; the afternoon is divided into  $T = 26$  time intervals of approximately 6 minutes. For each time interval we construct an undirected unweighted graph  $G^{(t)}$ , where the  $\mathbf{n} = 232$  nodes correspond to the students in the 10 classes.

The morning barycentre graph is computed using the  $T = 35$  graphs associated with the morning period. The afternoon barycentre graph is determined using the  $T = 26$  afternoon graphs. We display in Fig. 10-left the graph

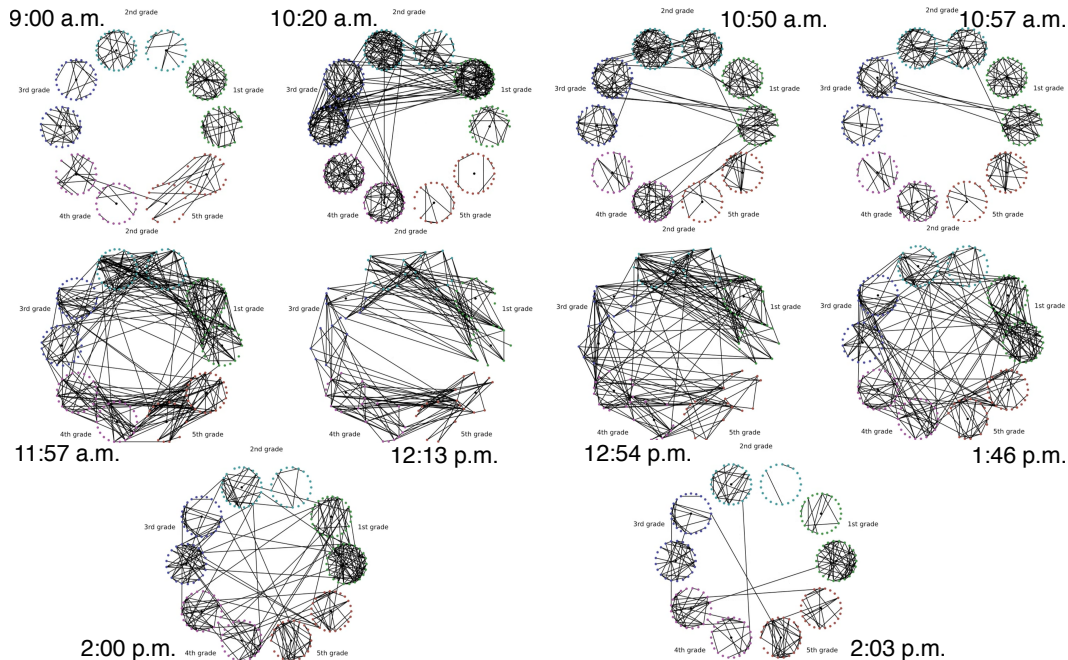


Figure 9: Top to bottom, left to right: snapshots of the face-to-face contact graph at times (shown next to each graph) surrounding significant topological changes.

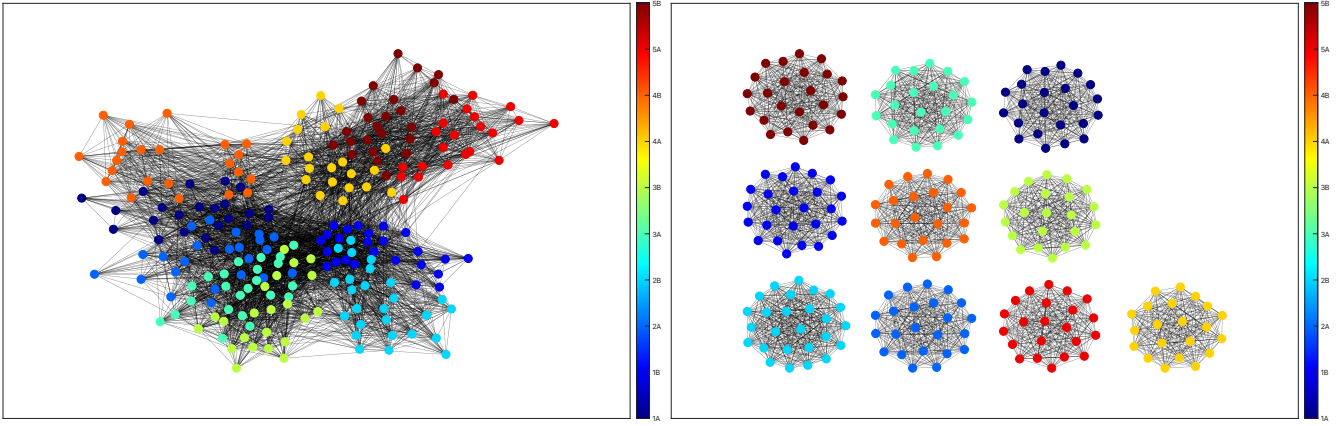


Figure 10: Morning period. Left: graph of the sample mean adjacency matrix  $\widehat{E}_T[\mathbb{P}]$  computed over the morning period; right: barycentre graph  $\widehat{\mu}_T^M[\mathbb{P}]$  computed over the morning period.

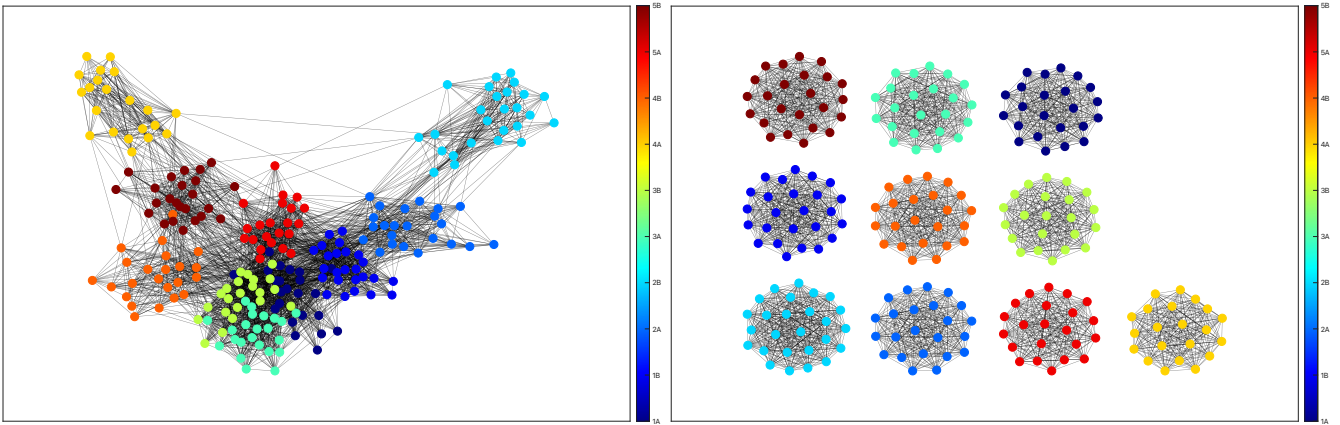


Figure 11: Afternoon period. Left: graph of the sample mean adjacency matrix  $\widehat{E}_T[\mathbb{P}]$  computed over the afternoon period; right: barycentre graph  $\widehat{\mu}_T^M[\mathbb{P}]$  computed over the afternoon period.

associated with the sample mean adjacency matrix  $\widehat{E}_T[\mathbb{P}]$ . We observe that the events such as lunchtime and recess trigger significant increases in the number of links between the communities, and disrupt the community structure (see Fig. 9). As a result the community structure associated with the individual classes collapses in the graph constructed from  $\widehat{E}_T[\mathbb{P}]$ , both for the morning and afternoon periods (see Fig. 10-left, and Fig. 11-left). In comparison, the barycentre graph, which does not rely on the presence or absence of edges, is able to recover the individual classes (see Fig. 10-right, and Fig. 11-right). Figure 2, which was displayed in Section 1.8, displays the histogram of all the eigenvalues of  $\mathcal{L}$  integrated over the morning (left) and afternoon (right) periods. The ten lowest eigenvalues are separated from the bulk in the morning and afternoon distributions (see Fig. 2), which guarantees that the graph associated with these distributions will have a community structure. The separation is more noticeable during the morning since students spend more time in their classroom during this period.

## 7 Discussion

In this work, we address the following question: when one computes a barycentre graph using a spectral pseudo-distance, one needs a basis of eigenvectors to reconstruct the barycentre graph: the distance only yields the eigenvalues. This paper contains several original contributions: (1) we formally define a criterion for estimating the eigenvectors, (2) we devise an algorithm to estimate the eigenvectors using the library of Soules vectors, (3) we provide a theoretical justification for the algorithm (in the context of the analysis of balanced Stochastic Block Models), and (4) we conduct

experiments that suggest that the algorithm performs as expected beyond the ensemble of balanced stochastic block models. As many papers in the research area of data representation and analysis, this manuscript combines algorithms with theory, where the theory is sometimes developed in a more restricted framework.

This work opens the door to further studies. Our experiments suggest that the method works beyond the restricted scope of balanced SBM, and one should be able to prove that Algorithm 1 solves Eq. (13) when graphs are sampled from SBM  $(\mathbf{p}, \mathbf{q}, \mathbf{n})$ . A second extension concerns the application of Algorithm 1 to graphs that have different sizes. Because we work with the normalized graph Laplacian, one can always compare interpolate a discrete spectrum on the interval  $[0, 2]$ , making the comparison of two graphs of different size possible. Finally, the analysis of the performance of the algorithm with graphs sampled from the preferential attachment models [82, 9] would have a significant practical impact. While less is known about the eigenvalues of the normalized Laplacian [38, 34], the topology of the preferential attachment model (with the high-degree vertices) is frequently found in real world networks, and therefore this model is worthy of attention.

## Acknowledgments

The author is grateful to the anonymous reviewers for their insightful comments and suggestions that greatly improved the content and presentation of this manuscript.

## 8 Additional proofs

### 8.1 Proof of Lemma 5

We derive the proof of Lemma 5. In the process, we prove several technical lemmata.

#### 8.1.1 The tensor product $\boldsymbol{\psi}_l \boldsymbol{\psi}_l^\top$

**Lemma 6.** We choose  $\boldsymbol{\psi}_1 \stackrel{\text{def}}{=} \mathbf{n}^{-1/2} \mathbf{1}$ , and denote by  $\boldsymbol{\psi}_l$  the Soules vector returned by Algorithm 1 at level  $l$ . Let  $\text{supp}(\boldsymbol{\psi}_l) = [i_0, i_1]$ , and let  $i^*$  be the location of the split in  $[i_0, i_1]$  such that  $\boldsymbol{\psi}_l|_{[i_0, i^*]} > 0$  and  $\boldsymbol{\psi}_l|_{[i^*+1, i_1]} < 0$  (see Fig. 3). Then,

$$\boldsymbol{\psi}_l \boldsymbol{\psi}_l^\top(i, j) = \frac{1}{i_1 - i_0 + 1} \begin{cases} \frac{i_1 - i^*}{i^* - i_0 + 1} & \text{if } i_0 \leq i, j \leq i^*, \\ \frac{i^* - i_0 + 1}{i_1 - i^*} & \text{if } i^* + 1 \leq i, j \leq i_1, \\ -1 & \text{if } \begin{cases} i_0 \leq i \leq i^*, & i^* + 1 \leq j \leq i_1, \\ i^* + 1 \leq i \leq i_1, & i_0 \leq j \leq i^*, \end{cases} \\ 0 & \text{otherwise.} \end{cases} \quad (41)$$

*Proof.* The proof is an elementary calculation based on the definition of  $\boldsymbol{\psi}_l$  given by Eq. (27), and the observation that  $\boldsymbol{\psi}_1(i) = \mathbf{n}^{-1/2}$ . Indeed, we know from Eq. (27) that  $\boldsymbol{\psi}_l$  is piecewise constant, and given by

$$\boldsymbol{\psi}_l(i) = \frac{1}{\sqrt{i_1 - i_0 + 1}} \begin{cases} \frac{\sqrt{i_1 - i^*}}{\sqrt{i^* - i_0 + 1}} & \text{if } i_0 \leq i \leq i^*, \\ -\frac{\sqrt{i^* - i_0 + 1}}{\sqrt{i_1 - i^*}} & \text{if } i^* + 1 \leq i \leq i_1, \\ 0 & \text{otherwise.} \end{cases} \quad (42)$$

The computation of the tensor product is immediate and yields the advertised result.  $\square$

### 8.1.2 The matrix $\sum_{k=1}^M \boldsymbol{\psi}_k \boldsymbol{\psi}_k^T$

In the following corollary, we describe the matrix  $\sum_{k=1}^M \boldsymbol{\psi}_k \boldsymbol{\psi}_k^T$ . When combined with Lemma 9, we use this corollary to reconstruct the geometry of the blocks in the SBM.

**Corollary 2.** *Let  $\{J_m\}$  be the  $M$  leaves in the binary Soules tree (these are intervals that are no longer split) after  $M$  steps of Algorithm 1. Then  $E_M \stackrel{\text{def}}{=} \sum_{k=1}^M \boldsymbol{\psi}_k \boldsymbol{\psi}_k^T$  is equal to*

$$e_M(\mathbf{i}, \mathbf{j}) = \begin{cases} \frac{1}{|J_m|} & \text{if } (\mathbf{i}, \mathbf{j}) \in J_m \times J_m, \\ 0 & \text{otherwise.} \end{cases} \quad (43)$$

Also,

$$\begin{cases} \sum_{k=2}^M \boldsymbol{\psi}_k \boldsymbol{\psi}_k^T(\mathbf{i}, \mathbf{j}) > 0 & \text{if } \exists m \in \{1, 2, \dots, M\}, (\mathbf{i}, \mathbf{j}) \in J_m \times J_m, \\ \sum_{k=2}^M \boldsymbol{\psi}_k \boldsymbol{\psi}_k^T(\mathbf{i}, \mathbf{j}) < 0 & \text{otherwise} \end{cases} \quad (44)$$

*Proof.* We first observe that after  $M$  iterations of Algorithm 1 there are  $M$  intervals  $J_m$  that are not split (the leaves in the binary tree shown in Fig. 4, where we count the construction of  $\boldsymbol{\psi}_1$  as the first iteration of the algorithm ( $M = 1$ )). This can be proved by induction, after observing that an iteration of Algorithm 1, described by Eq. (27), turns exactly one leaf in the tree into two leaves.

Next, we prove that  $\sum_{k=1}^M \boldsymbol{\psi}_k \boldsymbol{\psi}_k^T$  is nonnegative on each  $J_m \times J_m$ ,  $1 \leq m \leq M$ . Since, each interval  $J_m$  is a leaf of the tree, the interval  $J_m$  is not further decomposed, and there exists a vector  $\boldsymbol{\psi}_k$  such that  $\boldsymbol{\psi}_k|_{J_m} > 0$  or  $\boldsymbol{\psi}_k|_{J_m} < 0$  (see Fig. 4-right). We can therefore apply Lemma 6, with  $J_m = [i_0, i^*]$  or  $J_m = [i^*, i_1]$ , and  $\boldsymbol{\psi}_k \boldsymbol{\psi}_k^T$  is constant on  $J_m \times J_m$  (see Eq. (41)). All other larger scale (vectors  $\boldsymbol{\psi}_k$  such that  $J_m \subset \text{supp}(\boldsymbol{\psi}_k)$ ), also keep a constant value on  $J_m$ , and therefore  $\boldsymbol{\psi}_k \boldsymbol{\psi}_k^T$  is constant on  $J_m \times J_m$ . We conclude that  $\sum_{k=1}^M \boldsymbol{\psi}_k \boldsymbol{\psi}_k^T$  is constant on each  $J_m \times J_m$ ,  $1 \leq m \leq M$ .

We can then prove by induction that

$$e_M(\mathbf{i}, \mathbf{j}) = \begin{cases} \frac{1}{|J_m|} & \text{if } (\mathbf{i}, \mathbf{j}) \in J_m \times J_m, \\ 0 & \text{otherwise.} \end{cases} \quad (45)$$

For  $M = 1$  there is nothing to prove, since  $\boldsymbol{\psi}_1 = n^{-1/2} \mathbf{1}$ . Now, assume that Eq. (45) holds for  $M \geq 1$ , then  $E_{M+1} = E_M + \boldsymbol{\psi}_{M+1} \boldsymbol{\psi}_{M+1}^T$ , and  $\boldsymbol{\psi}_{M+1}$  is created by splitting an interval  $J_q$ ,  $1 \leq q \leq M$ , such that  $\text{supp}(\boldsymbol{\psi}_{M+1}) = J_q$ , and  $\boldsymbol{\psi}_{M+1}|_{J_m} = 0$  for all  $m \neq q$ . Since  $J_q$  is the only block that changes when going from  $M$  to  $M + 1$ ,  $\sum_{k=1}^{M+1} \boldsymbol{\psi}_k \boldsymbol{\psi}_k^T$  is equal to  $\sum_{k=1}^M \boldsymbol{\psi}_k \boldsymbol{\psi}_k^T$  on all the other blocks. Using the induction hypothesis, we then have for all  $m \neq q$ ,

$$\forall (\mathbf{i}, \mathbf{j}) \in J_m \times J_m, \quad e_{M+1}(\mathbf{i}, \mathbf{j}) = e_M(\mathbf{i}, \mathbf{j}) = \frac{1}{|J_m|}. \quad (46)$$

We are left with the computation of  $\sum_{k=1}^{M+1} \boldsymbol{\psi}_k \boldsymbol{\psi}_k^T$  on  $J_q \times J_q$ . Let us define  $i_0$  and  $i_1$  such that  $J_q = [i_0, i_1]$ , and let  $i^*$  be the index where  $J_q$  is split,  $J_q = [i_0, i^*] \cup [i^* + 1, i_1]$ . Then using Lemma 6 we have for all  $(\mathbf{i}, \mathbf{j}) \in J_q \times J_q$ ,

$$\boldsymbol{\psi}_{M+1} \boldsymbol{\psi}_{M+1}^T(\mathbf{i}, \mathbf{j}) = \frac{1}{i_1 - i_0 + 1} \begin{cases} \frac{i_1 - i^*}{i^* - i_0 + 1} & \text{if } (\mathbf{i}, \mathbf{j}) \in [i_0, i^*] \times [i_0, i^*], \\ \frac{i^* - i_0 + 1}{i_1 - i^*} & \text{if } (\mathbf{i}, \mathbf{j}) \in [i^* + 1, i_1] \times [i^* + 1, i_1], \\ -1 & \text{otherwise.} \end{cases} \quad (47)$$

From the induction hypothesis, we have for all  $(i, j) \in J_q \times J_q$ ,  $e_M(i, j) = |i_1 - i_0 + 1|^{-1}$ . Adding  $\sum_{k=1}^M \boldsymbol{\psi}_k \boldsymbol{\psi}_k^T$  and  $\boldsymbol{\psi}_{M+1} \boldsymbol{\psi}_{M+1}^T$  yields for all  $(i, j) \in J_q \times J_q$ ,

$$e_{M+1}(i, j) = \begin{cases} \frac{1}{i^* - i_0 + 1} & \text{if } (i, j) \in [i_0, i^*] \times [i_0, i^*], \\ \frac{1}{i_1 - i^*} & \text{if } (i, j) \in [i^* + 1, i_1] \times [i^* + 1, i_1], \\ 0 & \text{otherwise,} \end{cases} \quad (48)$$

which concludes the case for  $M + 1$ . By induction, Eq. (45) holds for all  $M$ .

We conclude the proof of Corollary 2 by proving Eq. (44). Let  $i, j$  be two nodes in the leaf  $J_q$  then  $e_M(i, j) = |J_q|^{-1}$ . Also,  $\boldsymbol{\psi}_1 \times \boldsymbol{\psi}_1(i, j) = n^{-1}$ , and thus

$$\sum_{m=2}^M \boldsymbol{\psi}_m \boldsymbol{\psi}_m^T(i, j) = \frac{1}{|J_q|} - \frac{1}{n} > 0, \quad (49)$$

since  $|J_q| > 1$ . Now, if  $(i, j)$  is not in any blocks  $J_q \times J_q$ , then  $e_M(i, j) = 0$ , and therefore  $e_M(i, j) - \boldsymbol{\psi}_1 \times \boldsymbol{\psi}_1(i, j) = -n^{-1} < 0$ .  $\square$

We now prove a series of lemmata that address the performance of Algorithm 1 and its ability to detect the blocks of a general SBM  $(\mathbf{p}, \mathbf{q}, \mathbf{n})$  by aligning the successive  $\boldsymbol{\psi}_m$  with the block boundaries. The proof hinges on the study of one iteration of Algorithm 1, as explained in Lemma 7.

### 8.1.3 One iteration of Algorithm 1

The next lemma studies a single iteration of Algorithm 1, which leads to the construction of the Soules vector  $\boldsymbol{\psi}_l$ . We assume that  $\text{supp}(\boldsymbol{\psi}_l) = [i_0, i_1]$ , and we consider the matrix  $\mathbf{P}$  that is nonzero only on  $[i_0, i_1] \times [i_0, i_1]$ , and is piecewise constant on two blocks  $J_0 \times J_0$  and  $J_1 \times J_1$ , where  $J_0 = [i_0, j]$ , and  $J_1 = [j + 1, i_1]$  (see Fig. 12),

$$\mathbf{P} = p_0(\mathbf{1}_{J_0} \mathbf{1}_{J_0}^T) + p_1(\mathbf{1}_{J_1} \mathbf{1}_{J_1}^T) + q(\mathbf{1}_{J_0} \mathbf{1}_{J_1}^T + \mathbf{1}_{J_1} \mathbf{1}_{J_0}^T). \quad (50)$$

We prove that in order to maximize  $|\langle \boldsymbol{\psi}_l \boldsymbol{\psi}_l^T, \mathbf{P} \rangle|^2$ , Algorithm 1 must always align  $i^*$  (the zero-crossing of  $\boldsymbol{\psi}_l$ ) with the jump in the SBM inside  $\text{supp}(\boldsymbol{\psi}_l \boldsymbol{\psi}_l^T)$  (see Fig. 12).

**Lemma 7.** *Let  $\boldsymbol{\psi}_l$  be the Soules vector returned by Algorithm 1 at level  $l$  with support  $\text{supp}(\boldsymbol{\psi}_l) \stackrel{\text{def}}{=} [i_0, i_1]$ . We consider the matrix  $\mathbf{P}$  that is nonzero only on  $[i_0, i_1] \times [i_0, i_1]$ , and is piecewise constant on two blocks  $J_0 \times J_0$  and  $J_1 \times J_1$ , where  $J_0 = [i_0, j]$ , and  $J_1 = [j + 1, i_1]$  (see Fig. 12),*

$$\mathbf{P} = p_0(\mathbf{1}_{J_0} \mathbf{1}_{J_0}^T) + p_1(\mathbf{1}_{J_1} \mathbf{1}_{J_1}^T) + q(\mathbf{1}_{J_0} \mathbf{1}_{J_1}^T + \mathbf{1}_{J_1} \mathbf{1}_{J_0}^T). \quad (51)$$

*Then,  $|\langle \boldsymbol{\psi}_l \boldsymbol{\psi}_l^T, \mathbf{P} \rangle|^2$  is maximum if the location of the zero-crossing of  $\boldsymbol{\psi}_l$  is equal to the location of the jump in the SBM,  $i^* = j$  (see Fig. 12).*

*Proof.* The proof relies on the computation of the inner-product between a Soules tensor product  $\boldsymbol{\psi}_l \boldsymbol{\psi}_l^T$  and an SBM whose support coincide with the support of  $\boldsymbol{\psi}_l \boldsymbol{\psi}_l^T$ . We use Lemma 6, and we study two cases for the choice of  $i^* \in [i_0, i_1]$ . We have

$$\langle \boldsymbol{\psi}_l \boldsymbol{\psi}_l^T, \mathbf{P} \rangle = p_0 \langle \boldsymbol{\psi}_l \boldsymbol{\psi}_l^T, \mathbf{1}_{J_0} \mathbf{1}_{J_0}^T \rangle + p_1 \langle \boldsymbol{\psi}_l \boldsymbol{\psi}_l^T, \mathbf{1}_{J_1} \mathbf{1}_{J_1}^T \rangle + q \langle \boldsymbol{\psi}_l \boldsymbol{\psi}_l^T, \mathbf{1}_{J_0} \mathbf{1}_{J_1}^T + \mathbf{1}_{J_1} \mathbf{1}_{J_0}^T \rangle. \quad (52)$$

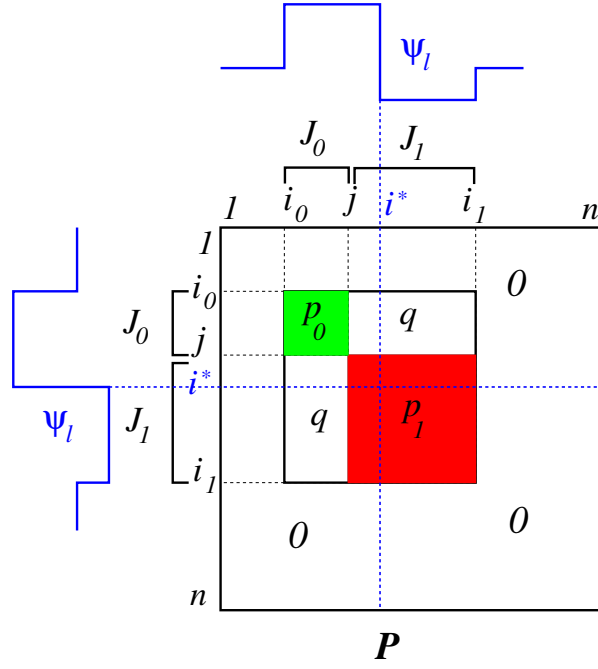


Figure 12: The vector  $\boldsymbol{\psi}_l$  (in blue) is created by splitting a block of indices  $[i_0, i_1]$  at level  $l-1$  into two sub-blocks,  $[i_0, i^*] \cup [i^*+1, i_1]$  at level  $l$ . We consider the matrix  $\mathbf{P}$  that is nonzero only on  $[i_0, i_1] \times [i_0, i_1]$ , and is piecewise constant on two blocks  $J_0 \times J_0$  (in green) and  $J_1 \times J_1$  (in red), where  $J_0 = [i_0, j]$ , and  $J_1 = [j+1, i_1]$

Also,  $\langle \boldsymbol{\psi}_l \boldsymbol{\psi}_l^T, \mathbf{1}_{J_q} \mathbf{1}_{J_r}^T \rangle = \langle \boldsymbol{\psi}_l, \mathbf{1}_{J_q} \rangle \langle \boldsymbol{\psi}_l, \mathbf{1}_{J_r} \rangle$ , for  $q, r \in \{0, 1\}$ . We define  $r_q \stackrel{\text{def}}{=} \langle \boldsymbol{\psi}_l, \mathbf{1}_{J_q} \rangle$  for  $q = 0, 1$ . Then

$$\langle \boldsymbol{\psi}_l = \boldsymbol{\psi}_l^T, \mathbf{P} \rangle = p_0 r_0^2 + 2q r_0 r_1 + p_1 r_1^2. \quad (53)$$

The expression of the coefficients  $r_0$  and  $r_1$  can be derived by using Eq. (42). We give the details for the computation of  $r_0$ , the computation of  $r_1$  is very similar. To compute  $r_0$ , we need to consider the two cases,  $i_0 \leq i^* \leq j$  and  $j \leq i^* \leq i_1$ . We recall from Eq. (42) that we always have

$$\boldsymbol{\psi}_l(i) = \frac{1}{\sqrt{i_1 - i_0 + 1}} \begin{cases} \frac{\sqrt{i_1 - i^*}}{\sqrt{i^* - i_0 + 1}} & \text{if } i_0 \leq i \leq i^*, \\ -\frac{\sqrt{i^* - i_0 + 1}}{\sqrt{i_1 - i^*}} & \text{if } i^* + 1 \leq i \leq i_1, \\ 0 & \text{otherwise.} \end{cases} \quad (54)$$

If  $i^* \leq j$  then  $\boldsymbol{\psi}_l$  changes sign over  $J_0$  and we have

$$\begin{aligned} r_0 = \langle \boldsymbol{\psi}_l, \mathbf{1}_{J_0} \rangle &= \frac{1}{\sqrt{i_1 - i_0 + 1}} \left\{ \sum_{i=i_0}^{i^*} \frac{\sqrt{i_1 - i^*}}{\sqrt{i^* - i_0 + 1}} - \sum_{i=i^*+1}^j \frac{\sqrt{i^* - i_0 + 1}}{\sqrt{i_1 - i^*}} \right\} \\ &= \sqrt{\frac{(i^* - i_0 + 1)(i_1 - i^*)}{i_1 - i_0 + 1}} \left( \frac{i_1 - j}{i_1 - i^*} \right). \end{aligned} \quad (55)$$

If  $j \leq i^*$  then  $\boldsymbol{\psi}_l$  is positive over  $J_0$  (this is the case for Fig. 12) and we have

$$r_0 = \langle \boldsymbol{\psi}_l, \mathbf{1}_{J_0} \rangle = \frac{1}{\sqrt{i_1 - i_0 + 1}} \sum_{i=i_0}^j \frac{\sqrt{i_1 - i^*}}{\sqrt{i^* - i_0 + 1}} = \sqrt{\frac{(i^* - i_0 + 1)(i_1 - i^*)}{i_1 - i_0 + 1}} \left( \frac{j - i_0 + 1}{i^* - i_0 + 1} \right). \quad (56)$$

A similar calculation yields  $r_1$ . If  $i^* + 1 \leq j + 1$  then  $\psi_l$  is negative over  $J_1$  and we have

$$r_1 = -\sqrt{\frac{(i^* - i_0 + 1)(i_1 - i^*)}{i_1 - i_0 + 1}} \left( \frac{i_1 - j}{i_1 - i^*} \right), \quad (57)$$

and if  $j + 1 \leq i^* + 1$  (this is the case for Fig. 12) then  $\psi_l$  changes sign over  $J_1$  and we have

$$r_1 = -\sqrt{\frac{(i^* - i_0 + 1)(i_1 - i^*)}{i_1 - i_0 + 1}} \left( \frac{j - i_0 + 1}{i^* - i_0 + 1} \right). \quad (58)$$

We are now ready to evaluate  $\langle \psi_l \psi_l^\top, \mathbf{P} \rangle = p_0 r_0^2 + 2q r_0 r_1 + p_1 r_1^2$ . Again, we need to consider the following two cases. If  $i^* \leq j$  then

$$\begin{aligned} \langle \psi_l \psi_l^\top, \mathbf{P} \rangle &= p_0 \frac{(i^* - i_0 + 1)(i_1 - i^*)}{i_1 - i_0 + 1} \left( \frac{i_1 - j}{i_1 - i^*} \right)^2 + p_1 \frac{(i^* - i_0 + 1)(i_1 - i^*)}{i_1 - i_0 + 1} \left( \frac{i_1 - j}{i_1 - i^*} \right)^2 \\ &\quad - 2q \frac{(i^* - i_0 + 1)(i_1 - i^*)}{i_1 - i_0 + 1} \left( \frac{i_1 - j}{i_1 - i^*} \right)^2 \\ &= \frac{(i^* - i_0 + 1)(i_1 - i^*)}{i_1 - i_0 + 1} \left( \frac{i_1 - j}{i_1 - i^*} \right)^2 \{p_0 + p_1 - 2q\}, \end{aligned} \quad (59)$$

which is maximum when  $i^* = j$ . In the case where if  $j \leq i^*$  we have

$$\langle \psi_l \psi_l^\top, \mathbf{P} \rangle = \frac{(i^* - i_0 + 1)(i_1 - i^*)}{i_1 - i_0 + 1} \left( \frac{j - i_0 + 1}{i^* - i_0 + 1} \right)^2 \{p_0 + p_1 - 2q\}, \quad (60)$$

which is also maximum when  $i^* = j$ . This concludes the proof that  $\langle \psi_l \psi_l^\top, \mathbf{P} \rangle$  is maximal if  $i^* = j$ .  $\square$

Lemma 8 extends Lemma 7 to the general edge probability matrix  $\mathbf{P}$  of an SBM (see Eq. (33)); it is used to prove Lemma 9 by induction. Lemma 8 can be proved using a proof by contradiction (using Lemma 7).

**Lemma 8.** *Let  $\mathbf{P}$  be the population mean adjacency matrix of SBM  $(\mathbf{p}, \mathbf{q}, \mathbf{n})$  defined by*

$$\mathbf{P} = \sum_{m=1}^M (p_m - q) \mathbf{1}_{B_m} \mathbf{1}_{B_m}^\top + q \mathbf{J}, \quad (61)$$

where the  $M$  blocks  $\{B_m\}$  form a partition of  $[\mathbf{n}]$ . Then, the split that creates  $\psi_2$  in Algorithm 1, is always located at the boundary between two blocks  $B_m$  and  $B_{m+1}$ .

*Proof.* Let  $i^*$  be the index associated with the construction of  $\psi_2$  and the subdivision of  $[\mathbf{n}]$ . We need to prove that  $i^*$  coincides with the endpoint of a block  $B_m$ . By contradiction, if  $i^*$  does not correspond to the boundary between two blocks, then there exists  $i_0 < i_1$  such that  $B_m = [i_0, i_1]$  and  $i_0 < i^* < i_1$ . Since  $\mathbf{P}$  is constant over the block  $[i_0, i_1] \times [i_0, i_1]$  (see Fig. 12 with  $p_0 = p_1 = q$ ), Lemma 7 tells us that the value of  $\mathbf{P}$  in  $B_m \times B_m$  does not contribute to  $|\langle \psi_2 \psi_2^\top, \mathbf{P} \rangle|^2$ , and Algorithm 1 should not have placed  $i^*$  in  $B_m$ .  $\square$

#### 8.1.4 $M$ iterations of Algorithm 1

This last lemma guarantees that after  $M$  iterations of Algorithm 1, the matrix  $\sum_{k=1}^M \psi_k \psi_k^\top$  associated with the first  $M$  Soules vectors recovers the block geometry. Lemma 9 is proved by induction on  $M$ , using Lemma 8.

**Lemma 9.** *Let  $\mathbf{P}$  be the population mean adjacency matrix of SBM  $(\mathbf{p}, \mathbf{q}, \mathbf{n})$  defined by*

$$\mathbf{P} = \sum_{m=1}^M (p_m - q) \mathbf{1}_{B_m} \mathbf{1}_{B_m}^\top + q \mathbf{J}. \quad (62)$$

Let  $J_l, 1 \leq l \leq M$  be the leaves in the binary Soules tree (these are intervals that are no longer split) after  $M$  steps of Algorithm 1. Then, the  $M$  blocks  $\{B_m\}$  in Eq. (62) coincide with the  $M$  intervals  $\{J_l\}$  discovered by Algorithm 1.

*Proof.* We prove the result by induction on  $M$ . If  $M = 1$ , there is nothing to prove. If  $M = 2$ , then Lemma 8 shows that  $\boldsymbol{\psi}_2$  recovers the block geometry. We assume that the result holds for all matrices  $\mathbf{P}$  with  $\mathbf{m} \leq M$  blocks that are given by Eq. (62). We consider the population mean adjacency matrix  $\mathbf{Q}$  defined by

$$\mathbf{Q} = \sum_{m=1}^{M+1} (\mathbf{p}_m - \mathbf{q}) \mathbf{1}_{C_m} \mathbf{1}_{C_m}^T + \mathbf{q} \mathbf{J}, \quad (63)$$

where  $\cup_{m=1}^{M+1} C_m = [n]$ . Because of Lemma 8, the first split of  $[n]$ , which leads to the construction of  $\boldsymbol{\psi}_2$  is aligned with the boundary of a block  $C_{m_0} = [i_0, i^*]$ . Without loss of generality, we can assume that the cut is aligned with the endpoint of  $C_{m_0}$ . We can then partition  $\mathbf{Q} = \mathbf{Q}_1 + \mathbf{Q}_2$ , where

$$\mathbf{Q}_1 = \sum_{m=1}^{i^*} (\mathbf{p}_m - \mathbf{q}) \mathbf{1}_{C_m} \mathbf{1}_{C_m}^T + \mathbf{q} \mathbf{1}_{[i^*]} \mathbf{1}_{[i^*]}^T \quad (64)$$

and

$$\mathbf{Q}_2 = \sum_{m=i^*+1}^{M+1} (\mathbf{p}_m - \mathbf{q}) \mathbf{1}_{C_m} \mathbf{1}_{C_m}^T + \mathbf{q} \mathbf{1}_{\{i^*+1, \dots, n\}} \mathbf{1}_{\{i^*+1, \dots, n\}}^T. \quad (65)$$

Again, because of Lemma 8, the next splits happen (independently) in  $\mathbf{Q}_1$ , or  $\mathbf{Q}_2$ . We can use the induction hypothesis to argue that all further splits will be located along the blocks in  $\mathbf{Q}_1$ , or  $\mathbf{Q}_2$ . After  $M$  splits, the algorithm has detected all  $M + 1$  blocks. By induction, the result holds for all  $M$ .  $\square$

Lemma 5 is then a direct consequence of Lemma 9 and Corollary 2.

## References

- [1] Abbe, E.: Community detection and stochastic block models: recent developments. *Journal of Machine Learning Research* **18**(177), 1–86 (2018)
- [2] Agterberg, J., Cape, J.: An overview of asymptotic normality in stochastic blockmodels: Cluster analysis and inference. *arXiv preprint arXiv:2305.06353* (2025)
- [3] Airoldi, E.M., Costa, T.B., Chan, S.H.: Stochastic blockmodel approximation of a graphon: Theory and consistent estimation. In: *Advances in Neural Information Processing Systems*. pp. 692–700 (2013)
- [4] Ferraz de Arruda, G., Tizzani, M., Moreno, Y.: Phase transitions and stability of dynamical processes on hypergraphs. *Communications Physics* **4**(1), 24 (2021)
- [5] Athreya, A., Cape, J., Tang, M.: Eigenvalues of stochastic blockmodel graphs and random graphs with low-rank edge probability matrices. *Sankhya A* pp. 1–28 (2022)
- [6] Avrachenkov, K., Dreveton, M.: *Statistical Analysis of Networks*. Now Publishers (2022)
- [7] Balan, R., Haghani, N., Singh, M.: Permutation invariant representations with applications to graph deep learning. *arXiv preprint arXiv:2203.07546* (2022)
- [8] Baldesi, L., Markopoulou, A., Butts, C.T.: Spectral graph forge: A framework for generating synthetic graphs with a target modularity. *IEEE/ACM Transactions on Networking* **27**(5), 2125–2136 (2019)
- [9] Barabási, A.L., Albert, R.: Emergence of scaling in random networks. *Science* **286**(5439), 509–512 (October 1999). <https://doi.org/10.1126.2025>
- [10] Blanchard, M., Jaffe, A.Q.: Fréchet mean set estimation in the Hausdorff metric, via relaxation. *Bernoulli* **31**(1), 432 – 456 (2025)

- [11] Borgs, C., Chayes, J.T., Cohn, H., Lovász, L.M.: Identifiability for graphexes and the weak kernel metric. In: Building Bridges II: Mathematics of László Lovász, pp. 29–157. Springer (2020)
- [12] Boumal, N., Mishra, B., Absil, P.A., Sepulchre, R.: Manopt, a matlab toolbox for optimization on manifolds. *The Journal of Machine Learning Research* **15**(1), 1455–1459 (2014)
- [13] Bovet, A., Delvenne, J.C., Lambiotte, R.: Flow stability for dynamic community detection. *Science advances* **8**(19), eabj3063 (2022)
- [14] Cencetti, G., Barrat, A.: Generating surrogate temporal networks from mesoscale building blocks. *Communications Physics* **8**(1), 159 (2025)
- [15] Chakrabarty, A., Chakraborty, S., Hazra, R.S.: Eigenvalues outside the bulk of inhomogeneous Erdős–Rényi random graphs. *Journal of Statistical Physics* **181**(5), 1746–1780 (2020)
- [16] Chaudhuri, K., Chung, F., Tsias, A.: Spectral clustering of graphs with general degrees in the extended planted partition model. In: Conference on Learning Theory. pp. 35–1. JMLR Workshop and Conference Proceedings (2012)
- [17] Chung, F.R.: Spectral Graph Theory. American Mathematical Society (1997)
- [18] Coifman, R., Geshwind, F., Meyer, Y.: Noiselets. *Applied and Computational Harmonic Analysis* **10**(1), 27–44 (2001)
- [19] Coifman, R., Lafon, S.: Diffusion maps. *Appl. Comput. Harmon. Anal.* **21**(1), 5–30 (2006)
- [20] Contisciani, M., Battiston, F., De Bacco, C.: Inference of hyperedges and overlapping communities in hypergraphs. *Nature communications* **13**(1), 7229 (2022)
- [21] D. Franco Saldaña, Y.Y., Feng, Y.: How many communities are there? *Journal of Computational and Graphical Statistics* **26**(1), 171–181 (2017)
- [22] Damle, A., Minden, V., Ying, L.: Simple, direct and efficient multi-way spectral clustering. *Information and Inference: A Journal of the IMA* **8**(1), 181–203 (2019)
- [23] Deng, S., Ling, S., Strohmer, T.: Strong consistency, graph laplacians, and the stochastic block model. *Journal of Machine Learning Research* **22**(117), 1–44 (2021)
- [24] Devriendt, K., Lambiotte, R., Van Mieghem, P.: Constructing Laplacian matrices with Soules vectors: inverse eigenvalue problem and applications. arXiv preprint arXiv:1909.11282 pp. 1–26 (2019)
- [25] Djurdjevac Conrad, N., Tonello, E., Zonker, J., Siebert, H.: Detection of dynamic communities in temporal networks with sparse data. *Applied Network Science* **10**(1), 1 (2025)
- [26] Doležal, M., Grebík, J., Hladký, J., Rocha, I., Rozhoň, V.: Relating the cut distance and the weak\* topology for graphons. *Journal of Combinatorial Theory, Series B* **147**, 252–298 (2021)
- [27] Donnat, C., Holmes, S.: Tracking network dynamics: A survey using graph distances. *The Annals of Applied Statistics* **12**(2), 971–1012 (2018)
- [28] Dubey, P., Müller, H.G.: Fréchet change-point detection. *The Annals of Statistics* **48**(6), 3312–3335 (2020)
- [29] Elsner, L., Nabben, R., Neumann, M.: Orthogonal bases that lead to symmetric nonnegative matrices. *Linear Algebra and its Applications* **271**(1-3), 323–343 (1998)
- [30] Eubanks, S., McDonald, J.J.: On a generalization of Soules bases. *SIAM journal on matrix analysis and applications* **31**(3), 1227–1234 (2010)

- [31] Failla, A., Cazabet, R., Rossetti, G., Citraro, S.: Describing group evolution in temporal data using multi-faceted events. *Machine Learning* **113**(10), 7591–7615 (2024)
- [32] Fan, J., Fan, Y., Han, X., Lv, J.: Asymptotic theory of eigenvectors for random matrices with diverging spikes. *Journal of the American Statistical Association* **117**(538), 996–1009 (2022)
- [33] Fan, X., Yue, Y., Sarkar, P., Wang, Y.X.R.: On hyperparameter tuning in general clustering problems. In: Proc. of the 37th Int. Conf. on Machine Learning. vol. 119, pp. 2996–3007 (2020)
- [34] Farkas, I.J.: Spectra of “real-world” graphs: Beyond the semicircle law. *Physical Review E* **64**(2) (2001). <https://doi.org/10.1103/PhysRevE.64.026704>
- [35] Faskowitz, J., Yan, X., Zuo, X.N., Sporns, O.: Weighted stochastic block models of the human connectome across the life span. *Scientific reports* **8**(1), 12997 (2018)
- [36] Ferguson, D., Meyer, F.G.: Theoretical analysis and computation of the sample Fréchet mean of sets of large graphs. *Information and Inference* **12**(3), 1347–1404 (03 2023)
- [37] Ferrer, M., Serratos, F., Sanfeliu, A.: Synthesis of median spectral graph. In: Pattern Recognition and Image Analysis. pp. 139–146 (2005)
- [38] Flaxman, A., Frieze, A., Fenner, T.: High degree vertices and eigenvalues in the preferential attachment graph. *Internet Mathematics* **2**(1), 1–19 (2005)
- [39] Gao, C., Lu, Y., Zhou, H.H.: Rate-optimal graphon estimation. *The Annals of Statistics* **43**(6), 2624–2652 (2015)
- [40] Garner, C., Lerman, G., Zhang, S.: Spectrally constrained optimization. *Journal of Scientific Computing* **100**(3), 89 (2024)
- [41] Gauvin, L., Panisson, A., Cattuto, C.: Detecting the community structure and activity patterns of temporal networks: a non-negative tensor factorization approach. *PloS one* **9**(1), e86028 (2014)
- [42] Gemmetto, V., Barrat, A., Cattuto, C.: Mitigation of infectious disease at school: targeted class closure vs school closure. *BMC infectious diseases* **14**, 1–10 (2014)
- [43] Génois, M., Barrat, A.: Can co-location be used as a proxy for face-to-face contacts? *EPJ Data Science* **7**(1), 1–18 (2018)
- [44] Gerlach, M., Peixoto, T.P., Altmann, E.G.: A network approach to topic models. *Science advances* **4**(7), eaaq1360 (2018)
- [45] Ghoshdastidar, D., Gutzeit, M., Carpentier, A., Von Luxburg, U.: Two-sample hypothesis testing for inhomogeneous random graphs. *The Annals of Statistics* **48**(4), 2208–2229 (2020)
- [46] Ginestet, C.E., Li, J., Balachandran, P., Rosenberg, S., Kolaczyk, E.D.: Hypothesis testing for network data in functional neuroimaging. *The Annals of Applied Statistics* **11**(2), 725–750 (2017)
- [47] Haasler, I., Frossard, P.: Bures-Wasserstein means of graphs. In: International Conference on Artificial Intelligence and Statistics. pp. 1873–1881. PMLR (2024)
- [48] Haghani, N., Singh, M., Balan, R.: Graph regression and classification using permutation invariant representations. In: AAI/Graphs and more Complex structures for Learning and Reasoning Workshop (2022)
- [49] Han, X., Jiang, Z., Liu, N., Hu, X.: G-mixup: Graph data augmentation for graph classification. In: International Conference on Machine Learning. pp. 8230–8248. PMLR (2022)

- [50] Kolaczyk, E.D., Lin, L., Rosenberg, S., Walters, J., Xu, J.: Averages of unlabeled networks: Geometric characterization and asymptotic behavior. *The Annals of Statistics* **48**(1), 514–538 (2020)
- [51] Le, C.M., Levina, E., Vershynin, R.: Concentration of random graphs and application to community detection. In: *Proceedings of the International Congress of Mathematicians*. pp. 2925–2943. World Scientific (2018)
- [52] Lee, J., Gharan, S., Trevisan, L.: Multiway spectral partitioning and higher-order Cheeger inequalities. *Journal of the ACM* **61**(6), 37 (2014)
- [53] Lovász, L.: *Large networks and graph limits*, vol. 60. AMS Bookstore (2012)
- [54] Löwe, M., Terveer, S.: Hitting times for random walks on the stochastic block model. arXiv preprint arXiv:2401.07896 pp. 1–26 (2024)
- [55] Lu, L., Peng, X.: Spectra of edge-independent random graphs. *The Electronic Journal of Combinatorics* pp. P27–P27 (2013)
- [56] Lunagómez, S., Olhede, S.C., Wolfe, P.J.: Modeling network populations via graph distances. *Journal of the American Statistical Association* **116**(536), 2023–2040 (2021)
- [57] Meyer, F.G.: <https://github.com/francoismeyer/barycentre-network> (2025)
- [58] Meyer, F.G., Shen, X.: Perturbation of the eigenvectors of the graph Laplacian: Application to image denoising. *Applied and Computational Harmonic Analysis* **36**(2), 326–334 (2014)
- [59] Meyer, F.G.: When does the mean network capture the topology of a sample of networks? *Frontiers in Physics* **12**, 1–11 (2024)
- [60] Mossel, E., Neeman, J., Sly, A.: Belief propagation, robust reconstruction and optimal recovery of block models. In: *Conference on Learning Theory*. pp. 356–370. PMLR (2014)
- [61] Olhede, S.C., Wolfe, P.J.: Network histograms and universality of blockmodel approximation. *PNAS* **111**(41), 14722–14727 (2014)
- [62] Oliveira, R.I.: Concentration of the adjacency matrix and of the laplacian in random graphs with independent edges. arXiv preprint arXiv:0911.0600 (2009)
- [63] Penshuck, M., Brandes, U., Hamann, M., Lamm, S., Meyer, U., Safro, I., Sanders, P., Schulz, C.: Recent advances in scalable network generation 1. *Massive graph analytics* pp. 333–376 (2022)
- [64] Petersen, A., Müller, H.G.: Fréchet regression for random objects with euclidean predictors. *The Annals of Statistics* **47**(2), 691–719 (2019)
- [65] Redko, I., Sebban, M., Habrard, A.: Non-negative matrix factorization meets time-inhomogeneous markov chains. In: *OPT2020* (2020)
- [66] Rohe, K., Chatterjee, S., Yu, B.: Spectral clustering and the high-dimensional stochastic blockmodel. *The Annals of Statistics* pp. 1878–1915 (2011)
- [67] Sattar, N.S., Buluc, A., Ibrahim, K.Z., Arifuzzaman, S.: Exploring temporal community evolution: algorithmic approaches and parallel optimization for dynamic community detection. *Applied Network Science* **8**(1), 64 (2023)
- [68] Shen, X., Meyer, F.: Low-dimensional embedding of fMRI datasets. *Neuroimage* **41**(3), 886–902 (2008)
- [69] Shine, A., Kempe, D.: Generative graph models based on Laplacian spectra? In: *The World Wide Web Conference*. pp. 1691–1701. ACM (2019)

- [70] Soules, G.W.: Constructing symmetric nonnegative matrices. *Linear and Multilinear Algebra* **13**(3), 241–251 (1983)
- [71] Stehlé, J., Voirin, N., Barrat, A., Cattuto, C., Isella, L., Pinton, J.F., Quaghiotto, M., Van den Broeck, W., Régis, C., Lina, B., Vanhems, P.: High-resolution measurements of face-to-face contact patterns in a primary school. *PloS one* **6**(8), e23176 (2011)
- [72] Sturm, K.T.: Probability measures on metric spaces of nonpositive. *Heat kernels and analysis on manifolds, graphs, and metric spaces* **338**, 357 (2003)
- [73] Tang, M.: The eigenvalues of stochastic blockmodel graphs. arXiv preprint arXiv:1803.11551 (2018)
- [74] Thibeault, V., Allard, A., Desrosiers, P.: The low-rank hypothesis of complex systems. *Nature Physics* **20** (2), 294–302 (2024)
- [75] Thiele, C.M., Villemoes, L.F.: A fast algorithm for adapted time–frequency tilings. *Applied and Computational Harmonic Analysis* **3**(2), 91–99 (1996)
- [76] White, D., Wilson, R.C.: Spectral generative models for graphs. In: *ICIAP 2007*. pp. 35–42 (2007)
- [77] Wills, P., Meyer, F.G.: Metrics for graph comparison: a practitioner’s guide. *PLoS ONE* **15**(2), 1–54 (2020)
- [78] Xu, H., Luo, D., Carin, L., Zha, H.: Learning graphons via structured Gromov-Wasserstein barycenters. In: *Proceedings of the AAAI Conference on Artificial Intelligence*. vol. 35 (12), pp. 10505–10513 (2021)
- [79] Xu, J.: Rates of convergence of spectral methods for graphon estimation. In: *International Conference on Machine Learning*. pp. 5433–5442. PMLR (2018)
- [80] Yan, B., Sarkar, P., Cheng, X.: Provable estimation of the number of blocks in block models. In: *ICAIS*. pp. 1185–1194 (2018)
- [81] Young, J.G., St-Onge, G., Desrosiers, P., Dubé, L.J.: Universality of the stochastic block model. *Phys. Rev. E* **98**, 032309 (2018)
- [82] Yule, G.U.: A mathematical theory of evolution, based on the conclusion of dr. j. c. willis, f.r.s. *Philosophical Transactions of the Royal Society B*. **213**, 402–410 (1925)
- [83] Zambon, D., Alippi, C., Livi, L.: Change-point methods on a sequence of graphs. *IEEE Transactions on Signal Processing* **67**(24), 6327–6341 (2019)
- [84] Zhang, X., Nadakuditi, R.R., Newman, M.E.: Spectra of random graphs with community structure and arbitrary degrees. *Physical review E* **89**(4), 042816 (2014)